August 2018

AC-Impedance Investigations of Li-Ion Batteries with Wide Temperature Performance

Huainan Qu
University of Wisconsin-Milwaukee

AC-IMPEDANCE INVESTIGATIONS OF LI-ION BATTERIES WITH WIDE TEMPERATURE PERFORMANCE

by

Huainan Qu

A Thesis Submitted in

Partial Fulfillment of the

Requirements for the Degree of

Master of Science

in Engineering

at

The University of Wisconsin-Milwaukee

August 2018

ABSTRACT

AC-IMPEDANCE INVESTIGATIONS OF LI-ION BATTERIES WITH WIDE TEMPERATURE PERFORMANCE

by

Huainan Qu

The University of Wisconsin-Milwaukee, 2018
Under the Supervision of Professor Deyang Qu

Solid electrolyte interphase (SEI) of lithium-ion batteries in three electrode pouch cells was studied by using electrochemical impedance spectroscopy (EIS). Two kinds of electrolytes were used for the comparison purpose. Electrochemical impedance of individual electrodes and the full cell was measured in various state of aging, charge and temperature conditions. The equivalent circuit was identified through distribution of relaxation times (DRT), and then used to fit the impedance data. The results show that majority of the full cell impedance at -20℃ arises from anode SEI.

Keywords: lithium-ion battery, electrochemistry impedance spectroscopy, wide temperature, solid electrolyte interface, distribution of relaxation times

To

my family,

my colleges,

and especially Dr. Deyang Qu

TABLE OF CONTENTS

LIST OF FIGURES

LIST OF TABLES

LIST OF ABBREVIATIONS

NMC	Lithium nickel manganese cobalt oxide
EC	Ethylene carbonate
PC	Propylene carbonate
DEC	Diethyl carbonate
EMC	Ethyl methyl carbonate
DMC	Dimethyl carbonate
SEI	Solid electrolyte interphase
DOE	Design of experiments
VC	Vinylene carbonate
XRD	X-ray diffraction
STM	Scanning tunneling microscope
XPS	X-ray photoelectron spectroscopy
EIS	Electrochemistry impedance spectroscopy
CPE	Constant phase element
DRT	Distribution of relaxation times
SOC	State of charge
SEM	Scanning electron microscope

ACKNOWLEDGEMENTS

Many people have helped me throughout the writing of this thesis and all of them deserve my gratitude. I would like to firstly thank my supervisor and thesis advisor Professor Dr. Deyang Qu for providing the investigating idea and guidance. When I was stuck in the middle of the project, he was always there instructing me with his wealth of knowledge and guiding me towards a solution. I would also like to thank Dr. Dong Zheng, Dr. Janak Kafle and Dr. Joshua Harris. They assisted me with using equipment, fabricating cells and making chemicals at the beginning of my project. Also, during my experiments, they always provided me guidance on both the operation and the principle, which allowed my project to move forward smoothly.

I wish to thank Professor Benjamin Church and Professor Ilya Avdeev as my thesis defense committee members and their suggestions on my thesis and future works.

I would like to thank the Johnson Controls for their generous funding for the lab equipment and materials. I would also like to thank the members of my research group, Dr. Gongwei Wang, Dr. Yang Luo, Jingyu Si, Tianyao Ding, Caleb Abegglen, Gonzo Couto-Lain, Nicholas Nelsen and Ozan Emsun for their help with my experiments and thesis. Without their support, I could hardly finish this project on time.

Lastly, I wish to thank my family for their love and support of my studies.

1. Introduction

1.1. Background

A battery is an energy device that convert the energy stored in chemical bonds into electricity. The basic principle of a battery is that when the anode is oxidized, the electrons flow from anode terminal to cathode terminal, and are reduce at the cathode [1].

Battery research started in the early 19th century [2], developed in the 20th century and is still booming currently. In the 200-year period, different kinds of batteries, such as lead-acid, Zinc-Manganese and so forth, have respectively dominated the history of the battery industry. However, the application of lithium chemistry in energy storage has brought energy storage technology to a higher stage in the late 20th century. According to the location of lithium in the Periodic table, the light weight and high electrochemical potential make lithium an ideal anode material for batteries.

At its introduction, lithium metal was directly used as the anode. However, upon recharging the lithium metal anode, dendritic deposition would happen on the lithium metal electrode surface which led to safety issues and decreased the advantages of the lithium battery. So, people tried to find a lithium alloy to solve the dendritic problem. During the exploration, it was found that lithium ion can be stored in specially structured materials. Namely, when charging and discharging the battery, the lithium ions could intercalate into and extract out from the electrodes instead of growing and fusing at the surface of the electrodes [3].

1.2. Lithium-ion battery electrodes

The revolutionary research of lithium-ion batteries dates back to 1979 when the first intercalation of lithium into a graphite electrode was demonstrated by Samar Basu [4]. The stable intercalation structure, LiC_6, was observed in their experiment. In 1983, the reversible electrochemical intercalation of lithium in graphite was demonstrated [5]. In their work, the electrode reaction was predicted as:

$$LiC_6 \rightleftarrows Li_{1-x}C_6 + xLi^+ + xe^-$$

This reaction was proved later and commonly used for the graphite anode in lithium ion-battery. Although other anode materials such as silicon, lithium titanium oxide etc. have also been studied, the graphite anode is dominant in most commercial lithium-ion battery because of its high stability.

If the graphite is used for the anode, the cathode must be the source of lithium [3]. Significant research concerning lithium-based cathode materials for lithium-ion battery dates back to 1980 when lithium cobalt dioxide ($LiCoO_2$) was used in rechargeable lithium batteries by both Ned A. Godshall at Stanford University [6] and John Goodenough at Oxford University [7]. In their work, the $LiCoO_2$ is a stable cathode material that gave a voltage to 4 V when lithium metal was the anode. Moreover, according to their structural studies, the retention of the layered structure in $LiCoO_2$ was shown during the lithium extracting and intercalation.

Plenty of research on lithium-ion batteries has preceded the first commercial lithium-ion battery released by Sony in 1991 [3]. After its release, the demand and application of lithium-ion batteries have increased continuously; which nowadays covers from personal electronic devices to electric vehicles. At the early stage of research, graphite was used as the anode material, while

$LiCoO_2$ was the most widely used cathode material. Today, Graphite has proved a stable and efficient anode and is still the common anode material in commercial lithium-ion batteries. However, novel materials have been found for the cathode.

For example, in 2001, a great improvement in the cathode of lithium-ion batteries was the use of lithium nickel manganese cobalt oxide (NMC) and was patented by Zhonghua Lu and Jeff Dahn [8]. In Hiroshi Yoshizawa's work in 2007 [9], NMC was compared with $LiCoO_2$. The result showed NMC had robust thermal behavior under high power cycling, which means NMC is more competitive in some applications such as electric vehicles. In addition, the rechargeable capacity of NMC was observed to be higher than $LiCoO_2$ in their work. Nickel, manganese and cobalt are the three elements in NMC, the ratio of them typically is 1:1:1. In lithium-ion battery the chemical reaction is believed as,

$$\mathrm{Li}_{1-x}\mathrm{MO}_2 + x\mathrm{Li}^+ + xe^- \rightleftarrows \mathrm{LiMO}_2$$

Where M represents NMC. This unique combination is widely used in automotive application.

1.3. Lithium-ion battery electrolyte

Besides the electrodes, the electrolyte is an essential part in a lithium ion-battery. The electrolyte serves as the medium for charge transfer. In order to supply a sufficient conductivity, liquid electrolyte were the first choice for lithium-ion batteries [10].

1.3.1. Salts

In the liquid electrolyte, a lithium salt is dissolved. The salt provides the ions required for the transfer of charge between anode and cathode. Since the lithium ion has a small ionic radius,

most simple salts, such as LiCl, LiF, are not sufficiently soluble in the low dielectric media [11]. There is a limited selection of lithium salts that meet the minimum solubility requirement. Those qualified lithium salts can usually find to be complexed with anions. Those anions consist of a simple anion core while being stabilized by a Lewis acid agent. One of the most successful lithium salts is lithium hexafluorophosphate ($LiPF_6$). This salt is the most commonly used in today's commercially available lithium-ion batteries as well as the lithium-ion batteries used in laboratory research.

$LiPF_6$ has a lower dissociation constant than some other salts, such as lithium bis(trifluoromethanesulfonyl)imide (LiIm) [12], and a lower chemical stability than some salts, such as lithium trifluoromethanesulfonate (LiTf) [13] and LiIm. However, the latter two salts react with aluminum to cause severe corrosion, which prevents them from wide adoption in lithium-ion batteries (where the aluminum is commonly used as current collector) [14]. $LiPF_6$ is a relatively ideal option considering the balance of its properties.

1.3.2. Solvents

The other component in electrolyte is the solvent which dissolves the lithium salt to a sufficient concentration. Although water is well-known that its polar molecular structure makes it an ideal solvent, however, the strongly reducing anode and oxidizing cathode makes using water as the solvent as well as those solvents with active protons impossible. On the other hand, in order to dissolve sufficient amounts of lithium salt and meet the concentration requirement, the solvent molecule must have some polarity. As a result, some organic solvents with carbonyl groups can be used as solvents [10]. The typical organic solvents involve some cyclic carbonates such as ethylene carbonate (EC), and propylene carbonate (PC), and some linear carbonates

including diethylcarbonate (DEC), ethylmethyl carbonate (EMC), dimethyl carbonate (DMC) and so forth.

For a real lithium-ion battery, an electrolyte with a single-solvent recipe can hardly meet all the requirements. The reason is that the expecting properties often exhibit contradictory performances within any single solvent. For example, when pursuing high polar molecular structure for concentration purposes, the melting point is usually high and the low temperature behavior is unavoidably sacrificed. So, two or more solvent mixtures have been investigated and applied.

EC is known to have high melting point making it a solid at room temperature. In 1970 the melting point of EC was suppressed when 9% PC added by Scrosati et al [15]. Later, an EC based solvent was systematically investigated, and proved to be a key component to maintain the capacity of a lithium-ion battery for long cycling when compared with the previously used solvent, PC. However, the significant composition of EC was not established until 1990 when Dahn et al [16] investigated the fundamental effects of EC on lithium ion intercalation into a graphite anode. EC was found to be playing a positive role in capacity retention (cycle life). The EC molecules are reduced (at 1.5 V Li/Li^+) on the graphite anode surface during the first lithiation cycle to produce a thin solid film called the Solid Electrolyte Interphase Layer (SEI) thereby increasing the battery life. Parallelly, in 1990s, the linear carbonates were brought into researchers' eyesight. In 1994, a new formulation with EC and DMC mixed was proposed as high stability solvent by Tarascon et al [17]. Later, other linear carbonates were applied as co-solvents in EC based electrolytes, such as DEC in Doron Aurbach's work in 1995 [18], and EMC in Yair Ein-Ili's work in 1996 [19]. An electrolyte mixed with linear carbonates brought the performance of the lithium-ion battery to a higher stage. However, there is still room for

improvement, especially concerning the wide temperature behavior. The previous work in our group [20] was focused on an electrolyte mixture containing more than two solvents. EC, PC, EMC, DMC and DEC were mixed in various ratios using the statistical tool, design of experiments (DOE). The cycling performance was tested both in room temperature and low temperature. The best combination found through this high throughput screening was three times better at low temperature than the traditional combination containing only EC and EMC. This study is the continuity of the same work in more detail. This work is concentrated on investigating the mechanism behind the increased performance of one electrolyte over the other.

1.3.3. Additives

Even though the electrolyte's solvent combination was carefully designed to improve the performance of the lithium-ion battery, there was still some properties limiting the batteries performance. Instead of replacing the whole electrolyte, incorporating a small amount of new components, called additives, was used and showed to be an effective way to achieve some target properties [21].

One of the major purposes of adding additives in any electrolyte is to control the chemistry of the SEI. The additives generally get reduced on anode surface before EC is reduced and give a more stable SEI. Such additives include vinylene carbonate (VC), which is widely used in lithium-ion battery electrolyte. In 2011, a systematic study of VC was conducted by Xiong et al [22]. In their work, the influence of different VC concentrations from 0% to 3% by weight on the SEI formation at a graphite anode was investigated. It has been claimed that 1% VC contributes positively to the SEI formation without creating any significant negative results.

Another important purpose of additives is to stabilize the electrolyte system, especially at high temperatures. In 2002, a series of work was done by Xu et al. on the salt, lithium bis(oxalate)borate (LiBOB) [23]. Compared with $LiPF_6$, LiBOB gave a stable performance under high temperature cycling in their work. It was found that LiBOB had the capability to prevent the exfoliation of a graphite anode when using a PC based electrolyte [24]. In 2003, The mechanism of the improvement was investigated by Xu et al [25]. Xu et al observed that the BOB anions decomposed on the graphite anode, which indicated that it might assist in the stability of the SEI.

In the previous work performed in our group, it was also found that adding 0.5% of LiBOB by weight improved the cycling performance of lithium-ion batteries significantly [20].

1.4. Introduction of SEI

1.4.1. SEI formation

Lithium-ion battery electrolyte can be thought of as a kind of non-aqueous batter. It has been learned that in a non-aqueous electrolyte, while the metallic ions are accepting electrons at the surface of the alkali metal electrode, the electrons can also reduce the organic solvent. As mentioned above, the product of this reduction is a thin layer covering the surface of the electrode, and acting as a solid electrolyte, so called SEI. In early 1970, Dey et al. [26] observed and concluded that lithium metal in a non-aqueous system was covered by a lithium ion conducting layer. However, this layer was not well defined until Peled et al. first formally named it the SEI after investigating its chemical and physical properties in 1979 [27].

By summarizing the literature and calculations, Peled et al. [27] highlighted several significant properties of SEI in their paper. Firstly, the alkali metal electrode was covered by a

dense SEI with a thickness of 20 A to 40 A. Secondly, SEI was conductive for cation but insulating for electron. Governed by the Schottky vacancies mechanism, the cation migrated through the SEI and gained an electron from the metal at the electrode surface. Finally, even though the SEI was a good insulator for electrons, the thickness of SEI still increased with time of storage. This is because the inhomogeneous area was conductive towards electrons which would further reduce the solvent. As a result, the growing rate was significantly dependent on the homogeneity of the SEI formation.

The highly lithiated graphite possesses similar chemical properties as the lithium metal. However, the mechanism of SEI formation is much more complex at the graphite surface. One model to demonstrate the SEI formation on a graphite electrode was proposed by Besenhard et al. in 1995 [28]. It is called Besenhard model and is shown in Figure 1-1. Based on the experiment and the results of cyclic voltammetry, it was claimed that the solvated graphite-intercalation compounds were $Li(solv)_yC_n$. It was concluded that this compound had a rather short lifetime and the film was formed via the secondary reaction of the solvated compound. Moreover, according to the analysis, it was predicted that some of the electrolyte decomposition products were immobile and remained inside the graphite layer.

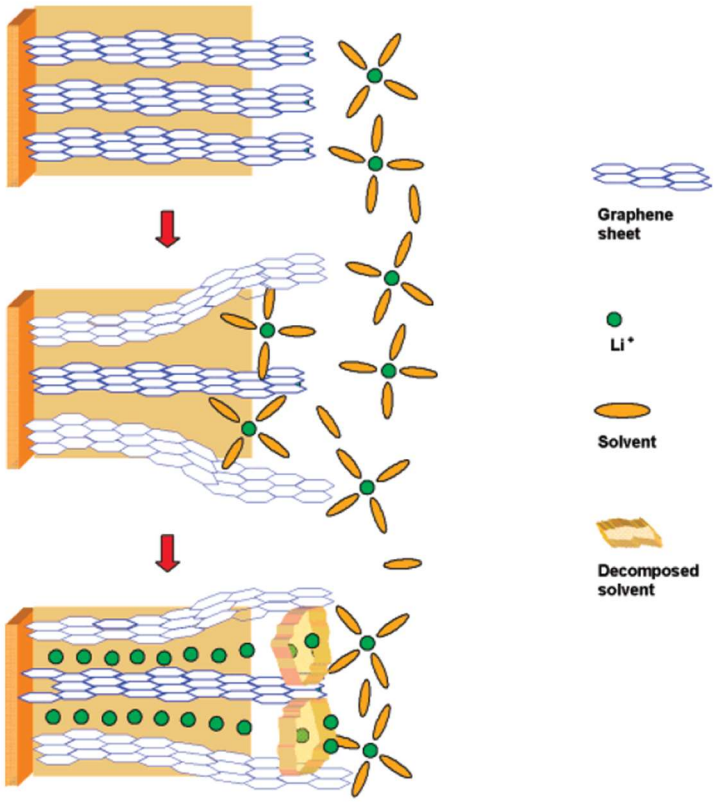

Figure 1-1 Besenhard model demonstrating SEI formation on graphite anode [10]

1.4.2. SEI detection

After Besenhard explained the uniqueness of the graphite electrode SEI formation, research was concentrated on finding the experimental evidence of the Besenhard model and on the relationship between the SEI formation process and its properties, which became the dominant focus. Moreover, with the development of surface detection technology, many advancements were made in the SEI research. For example, in 1997, Abe and Ogumi [29] identified solvated graphite-intercalation compounds using XRD. Similarly, with microscopic means, in 1996, Inaba et al. [30] applied STM and observed the formation of some products on the graphite surface during polarization. They explained it as solvent co-intercalation. However, in 1996, another explanation for SEI formation was demonstrated by Kanamura et al. XPS was applied in their

research and they concluded that the SEI possessed a multi layered structure [31]. Different detection methods helped researchers with understanding the formation process and the components of the SEI. But, for most of the methods, the battery has to be opened to perform SEI characterizing. The opening of the cells and the sample preparation could cause contamination of the surface and alteration of the SEI structure. Therefore, the SEI structure studied by *ex-situ* analysis might vary from sample to sample.

In 2000, electrochemical impedance spectroscopy (EIS) was conducted on graphite electrode by Chung et al. [32]. Comparing the EIS result from exfoliated graphite sample with the result from fresh sample, a significant increase in double-layer capacitance was observed in the exfoliated one. It was concluded that the rupture that caused the inhomogeneity was the reason of graphite electrode failure. EIS then became widely used in lithium-ion battery research.

1.5. Introduction of EIS

EIS has proved to be a powerful tool in electrochemistry research. In EIS, a sinusoid disturbance signal at different AC frequencies are applied to the battery. The response reflects the specific properties of the electrode material and the electrode surface. According to Ohm's law, if the excitation signal is voltage, the current signal will be the response. In contrast, if the input signal is current, the voltage signal will be the output. Then the electrode properties can be interpreted by calculating the impedance from the voltage and current data.

When a material is immersed in an electrolyte, because of the difference of Gibbs free energy between the electrode and the electrolyte, the chemical reaction leads to the reorientation of the charge particles and the formation of the double layer [33]. If no disturbance is introduced, it becomes a steady state eventually. However, when the disturbance induces electron flow, the

chemical reaction happens at the electrode surface and leads the system an unsteady state. Meanwhile, as the reaction produces and consumes particles, mass transfer happens in the electrolyte near the electrode surface, which is known as diffusion. In general, a double layer, chemical reaction and diffusion are the three-major processes on the electrode surface. All of them have a unique response to a sinusoid signal disturbance.

1.5.1. Mathematics

Since there are equivalent amount of positive and negative charges clustering parallel to the electrode surface, the double layer is supposed to behave as a traditional capacitor. However, the impedance of the double layer at the graphite surface is different from an ideal capacitor. It was observed that the capacitance is frequency dependent and the phase angle is independent of the double layer, while it is the opposite in ideal capacitor. In 1932, Frickee et al. [34] first reported the constant phase element (CPE) for modeling the double layer behavior. In 1994, Tamas Pajkossy et al. [35] demonstrated that the CPE depended strongly on the state of the surface of the electrode. By comparing the electrodes with varying degrees of roughness, it was believed that the deviation from the ideal capacitance resulted from the inhomogeneity of the electrode surface.

The impedance expression for the double layer, Z_{CPE}, was summarized by Conway [36] as,

$$Z_{\mathrm{CPE}} = \frac{1}{T(i\omega)^p} \tag{1-1}$$

Where T is the capacitance combined with the bulk resistance and p is a factor representing the divergence from the ideal capacitor.

In an electrochemical system, the chemical reaction on the electrode is governed by the Butler-Volmer equation. Taking the cathode electrode as an example, the current density I can be expressed as,

$$I = i^0 e^{-\frac{\alpha n F}{RT}(E-E^0)} \tag{1-2}$$

Where i^0 is the exchange current density, α is cathodic charge transfer coefficients, n is the number of moles of electrons, T is the temperature, E^0 is equilibrium potential, and E represents the potential of the electrode.

The Butler-Volmer equation gives the relationship between the operation voltage and current. Namely, it reflects the properties of the chemical reaction. A disturbance signal, ΔE,can be superimposed in the equation, and introduces the response, ΔI.

$$\Delta I = i^0 e^{-\frac{\alpha n F}{RT}(E+\Delta E-E^0)} - i^0 e^{-\frac{\alpha n F}{RT}(E-E^0)} \tag{1-3}$$

$$\therefore \Delta I = i^0 e^{-\frac{\alpha n F}{RT}(E-E^0)} \left(e^{-\frac{\alpha n F}{RT}(\Delta E)} - 1\right) \tag{1-4}$$

Obviously, this nonlinear equation makes the measurement difficult. According to the Maclaurin series of an exponential function,

$$e^x = 1 + x + \frac{x^2}{2!} + \cdots + \frac{x^n}{n!} \tag{1-5}$$

If the disturbance, ΔE, is small enough, the Butler-Volmer equation can be locally linearized as,

$$\Delta I = -i^0 e^{-\frac{\alpha n F}{RT}(E-E^0)} \frac{\alpha n F}{RT} \Delta E \tag{1-6}$$

In a similar way, if a small enough current is the input,

$$\Delta E = \frac{-RT \quad \left(\frac{\Delta I}{i^0} e^{\frac{\alpha nF}{RT}(E-E^0)} + 1\right)}{\alpha nF} \tag{1-7}$$

the equation can also be linearized based on the Maclaurin series of natural logarithm,

$$\ln(1-x) = -x - \frac{x^2}{2} - \cdots - \frac{x^n}{n} \tag{1-8}$$

The exactly same linearized relationship can be obtained. So, from this principle, no matter what the input signals are, as long as they are small enough to linearize the equation, the calculated impedance by current input or voltage input should be equivalent.

As a result, responding to a small enough excitation signal, the chemical reaction at the electrode and electrolyte interface behaves as a resistor R_F,

$$R_F = \frac{\Delta E}{\Delta I} = -e^{\frac{\alpha nF}{RT}(E-E^0)} \frac{RT}{i^0 \alpha nF} = const \tag{1-9}$$

In terms of the diffusion, the concentration C, and its distribution is governed by Fick's second law,

$$\frac{\partial C}{\partial t} = D\left(\frac{\partial^2 C}{\partial x^2}\right) \tag{1-10}$$

Where D is the diffusion coefficient.

At the electrode surface, it is assumed that the consumption or the production of the charges in the chemical reaction is reasonably compensated from or migrate to the bulk electrolyte. So, the boundary condition at electrode surface can be expressed as,

$$\left(\frac{\partial C}{\partial x}\right)_{x=0} = \frac{I}{nFD}\sin \omega t \tag{1-11}$$

In most cases, another boundary condition can be considered semi-infinite. Namely, the scale where the concentration gradient affects is far less than the scale of bulk electrolyte. Hence far from the electrode surface, the electrolyte concentration is close to the concentration of the bulk electrolyte, C^0. Then the boundary condition of another side can be expressed as,

$$C_{x=\infty} = C^0 \tag{1-12}$$

The Fick's second law equation can be solved [33],

$$C^0 - C = \frac{I}{nF\sqrt{\omega D}} e^{-\sqrt{\frac{2D}{\omega}}x} \sin\left(\omega t - \sqrt{\frac{2D}{\omega}}x - \frac{\pi}{4}\right) \tag{1-13}$$

The Nernst equation describes the relationship between the electrode potential and the concentration of the reactant.

$$\Delta E = \frac{RT}{nF}\ln\left(1 + \frac{\Delta C^S}{C^0}\right) \tag{1-14}$$

By applying a small enough disturbance, the change of the concentration at electrode surface is considered much smaller than that in the bulk.

$$\Delta E = \frac{RT\Delta C^S}{nFC^0} \tag{1-15}$$

Then, the impedance due to diffusion can be obtain [33].

$$Z_{\mathrm{D}} = \frac{RT}{n^2F^2C^0\sqrt{2\omega D}} - \frac{RT}{n^2F^2C^0\sqrt{2\omega D}}i \tag{1-16}$$

The Warburg impedance is defined in the expression,

$$\sigma = \frac{RT}{n^2F^2C^0\sqrt{2D}} \tag{1-17}$$

So,

$$Z_{\mathrm{D}} = \frac{\sigma}{\sqrt{\omega}}(1 - i) \tag{1-18}$$

In a lithium-ion battery, the semi-infinite boundary condition may not be perfectly satisfied because of the tightly packed particles. However, the semi-infinite Warburg element is still shown to be applicable and widely utilized in numerous lithium-ion battery impedance research. The work done by Guorong Hu et al. is one of these examples [37]. In their research, a novel cathode material was synthesized based on $LiFePO_4$ for a lithium-ion battery. When testing the battery with EIS, the semi-infinite Warburg element was applied to simulate the real data. The simulation result showed the fitting was perfect which indicated the semi-infinite Warburg element was applicable to in lithium-ion batteries.

1.5.2. Equivalent circuit

Since the electrochemical steps including double layer, chemical reaction and diffusion have a unique response to the sinusoid signal, they can be regarded as equivalent circuit elements. Then, either a single electrode or the whole battery is nothing more than the combination of multiple electrochemical steps. As a result, the EIS can be modeled by a series of equivalent circuit elements. The specific values in the circuit reflect the properties of the electrochemical steps in the battery.

Many researchers have focused on characterizing the lithium-ion battery using EIS. A systematic EIS investigation into lithium-ion batteries was done by Nagasubramanian et al. in 1999 [38]. They conducted the experiment by using both electrodes from a commercial lithium-

ion battery. EIS with a frequency range from 65kHz to 0.1Hz was taken in a two-electrode cell at 4.1V, 3.6V and 3.1V at different temperatures ranging from 35℃ to -40℃. EIS with the same frequency range was conducted in three-electrode cell only at 4.1V at 0℃ and -20℃. Without simulating the EIS data with an equivalent circuit, a direct summary from the result was the resistance of the cell grew significantly at low temperature. From the three-electrode cell result, they claimed that the growth came mostly from the cathode part. Later, in 2012, Tetsuya et al. [39] published a novel equivalent circuit for the EIS results of a two-electrode commercial lithium-ion battery. Three resistance and capacitor elements were included in their novel circuit to model the SEI, the anode and the cathode separately. EIS was taken at different states of charge. In their result, it was concluded that the novel equivalent circuit fit the experiment results perfectly. In the same year, an additional EIS study performed under different temperatures was conducted by the same group [40]. EIS with frequency range of 100kHz to 10mHz was applied to the same commercial lithium-ion battery at temperatures from 20℃ to -20℃. Applying their novel equivalent circuit, the EIS of a lithium-ion battery under a wide temperature range was investigated. At high temperatures, the impedance from various components were overlapping. However, at low temperature, each semicircle from SEI, anode and cathode could be separated in the Nyquist plot.

Besides characterizing the battery, EIS is also a powerful method in detailed investigation of the SEI. As mentioned previously, the SEI forms at the surface of electrode where the electrochemical phenomena take place. Since EIS analysis gives the properties of the electrochemical steps, SEI properties can be obtained from EIS analysis. In 2017, Miriam Steinhauer et al. [41] studied the SEI formation on a graphite anode with EIS. In their research, a graphite/Li two-electrode half-cell and the same three-electrode cell with Li as the reference

were investigated. The *in-situ* EIS was taken during the first charge and the second charge for both cells. Simulating with the equivalent circuit, they summarized the process of SEI formation.

1.5.3. Distribution of relaxation times

When analyzing the electrochemical processes of a battery with EIS, much of the existing work (as mentioned above) fits the impedance data with an empirical circuit or optimized circuit. However, due to the complexity of the system, directly fitting the Nyquist plot from the frequency domain impedance spectrum does not allow for the separation of the individual electrochemical process and makes the physical meaning of the results weak [42]. Therefore, in order to select the reasonable equivalent circuit, which reflects the genuine physical process, it is necessary to transfer the impedance in the frequency domain into a distribution of the impedance in the time domain. This technique is referred to as distribution of relaxation times (DRT).

In principle, a well-known electric system responding to a sinusoid signal can be modeled by a finite Voigt model which contains finite RC elements [43] (shown in Figure 1-2). Each RC elements represents a specific process. The total impedance depending on the frequency is the sum of the individual RC elements,

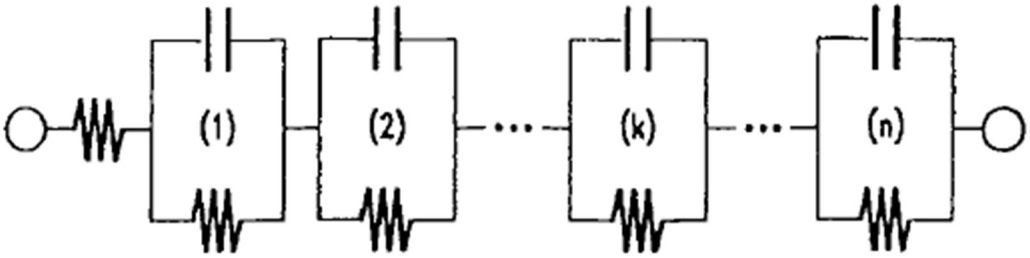

Figure 1-2 Voigt electrical circuit[43]

However, inside a battery, the number of processes is unknown. Instead of a finite Voigt model, an infinite Voigt model gives the distribution of the impedance along the relaxation time. It can be expressed as [44],

$$Z_{pol}(\omega) = R_{pol} \sum_{k=1}^{N} \frac{g_k}{1+iw\tau_k} = \sum_{k=1}^{N} \frac{R_k}{1+iw_{\ k}} \tag{1-19}$$

Where $Z_{pol}(\omega)$ is the impedance in frequency domain, R_k represents the relative share of the overall polarization resistance R_{pol} in vicinity of time-constant τ_k.

To demonstrate the DRT, a simple example with two processes is shown in Figure 1-3. In the finite model, each element has an impulse at their relaxation time. While in the infinite model, the process can be predicted from the peak of the continuous distribution. The location of the peak is the relaxation time. The height represents the impedance of the process and the width of the peak indicates the complexity of the process.

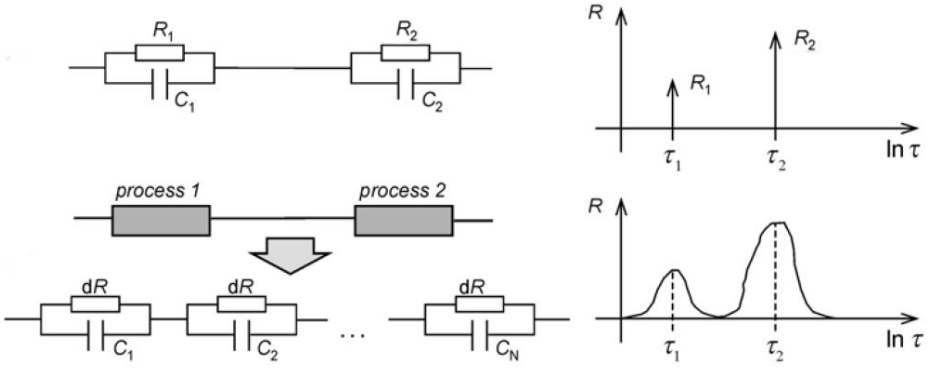

Figure 1-3 Demonstration of infinite RC elements model and distribution of relaxation times [42]

1.6. Remarks on this work

In our previous work, our group has developed an electrolyte which significantly improves the cycling performance of a lithium-ion battery, especially at low temperatures [20]. It was

believed that the SEI properties played a key role in the increased performance. However, the mechanism how the SEI affects the battery remains unclear. Therefore, this work aims to identify the relationship between SEI properties and the battery's performance. This work is predominantly based on EIS investigation. DRT is first applied on the EIS data. By analyzing the peaks in the DRT plot, the number of electrochemical processes is predicted. The equivalent circuit is fitted to the impedance at various frequency ranges to obtain numerical values of different processes.

Furthermore, the existing work on EIS based research shows the limitation of two-electrode impedance testing. Without an accurate theory to separate the full cell impedance into anode and cathode impedance individually, extracting the equivalent elements representing SEI, anode and cathode from the full cell EIS becomes unpersuasive. Many two-electrode EIS equivalent circuits were created based on some three-electrode experimental data. However, in most three-electrode cell experiments, a completely closed system cannot be maintained, which might introduce unknown factors which could disturb the result. We believe that taking EIS for an individual electrode in a three-electrode cell can reflect the genuine properties of electrochemical processes, also it may help to build up a theory for analyzing the EIS separation from a full cell.

2. Experiments

2.1. Sample preparations

2.1.1. Chemicals

$LiPF_6$, LiBOB and VC were purchased from Sigma Aldrich and used without further purification. The chemical's structure is shown in

Figure 2-1. EC, EMC and DMC were purchased from BASF Corporation Ohio and used without further treatments. For the NMC cathode, the loading of the active material was 6.80 mg/cm^2 on an aluminum foil current collector, and the reversible capacity is theoretically 0.93 mAh/cm^2. The graphite anode had 3.25 mg/cm^2 of active material loading on a copper foil current collector. Both the cathode and anode were prepared in house. Two pieces of lithium foil (0.625 inch in diameter, 0.2 mm in thickness) were used as the reference electrode. Celgard 2325 polymer was used as the separator.

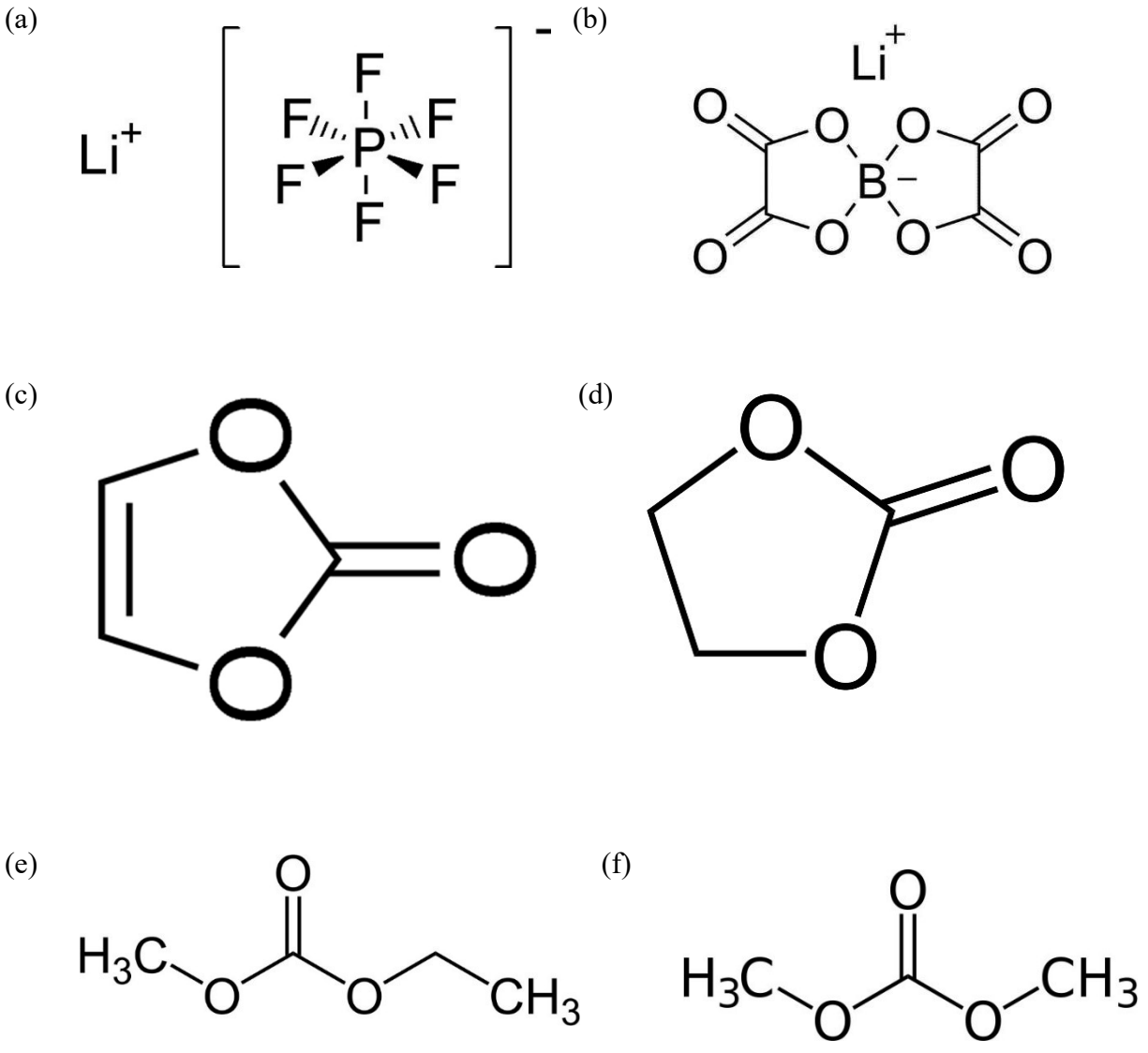

Figure 2-1 Structures of the electrolyte salt, additives and organic solvents in this experiment.

(a) LiPF6 (b) LiBOB (c) VC (d) EC (e) EMC (f) DMC

2.1.2. Electrolytes

Two types of electrolytes were used in this work. One is the best performing low temperature electrolyte that has been developed previously in our group. The other is the controlled electrolyte. For convenience the controlled electrolyte was called baseline electrolyte and another was called improved electrolyte. A mixture of 20.0 g of solvent combination (EC, EMC, DMC) at the desired ratio were prepared. The baseline electrolyte solvent has EC/EMC in ratio 3:7 (weight). The improved electrolyte contains solvent mixture EC, EMC and DMC in 5: 30: 65 ratios (weight). The lithium salt ($LiPF_6$) was added to each of the solvent composition to make a 1.0 M solution. In the improved electrolyte solution, 0.22 g of VC and 0.114 g of LiBOB was added to make 1 % and 0.5 % by weight of the total electrolyte. The mixture was left overnight to dissolve the salt and additives completely.

2.2. Cell fabrications

2.2.1. Coin cells

Two-electrode coin cells were made using each electrolyte for charge and discharge experiments. Circular pieces of anode (15.8 mm diameter) and cathode (14.3 mm inch diameter) were prepared for coin cell making. 50 μL of electrolyte was used in each coin cell. The crimped coin cells were taken out from the glove box and stored at 25℃ for 24 hours.

2.2.2. Pouch cells

Rectangular piece of cathode (140 mm * 73 mm, shown in Figure 2-2 (a)) and anode (142 mm * 77 mm, shown in Figure 2-2 (b)) were prepared for constructing pouch cells. The total theoretical capacity per cell is 95.05 mAh based on the cathode with 102.2 cm^2 total active area.

Lithium foil of 0.2 mm thickness and 15.8 mm diameter was used as the reference electrode. The reference electrode current collector was a copper foil and prepared in a specific shape shown in Figure 2-2 (c). The shape was designed to attach the lithium foils and position the reference in the middle of the cell.

The well-cut electrodes were dried at 80℃ and 0.2 atm for 12 hours in a vacuum oven (shown in Figure 2-2 (d)). Then the electrodes were welded to the terminal tabs in the dry room using an ultrasonic welding machine (shown in Figure 2-2 (e)). The nickel coated aluminum tab was welded to the cathode on its current collector (shown in Figure 2-2 (f)), and nickel coated copper tab was welded to the anode (shown in Figure 2-2 (g)), and reference electrode (shown in Figure 2-2 (h)).

The pouch cell was assembled in the glove box. The cathode and anode were separated by two pieces of separator (shown in Figure 2-3 (a)). Two pieces of lithium foil was pressed on to the reference electrode current collector (shown in Figure 2-3 (b)). The reference electrode was sandwiched between the two pieces of the separators (as shown in Figure 2-3 (c)).

The case of the pouch cell was composed of an aluminum laminated film coated with nylon purchased from MTI Corporation. The case is (180 mm * 226 mm) folded in the middle of the long edge. The folded edge was firstly sealed for 8 seconds at 185℃ using a vacuum sealing machine (shown in Figure 2-3 (d)). The sealing edge is 5 mm in width. The assembled three-electrode core was positioned in the case. The glue of the tabs was placed right at the top edge of the case. After sealing one of the side edges, the electrode's tab glue was sealed with the case along the top edge. After cooling in glove box for 5 minutes, 3.0 g of electrolyte was added into each of the pouch cells and spread uniformly. After the electrolyte was filled, the last side edge

was sealed. The whole sealing process was under a slight vacuum condition. A well-done pouch cell was shown in Figure 2-3 (e). After labeling the cell, it was left to rest at 25℃ for 24 hours.

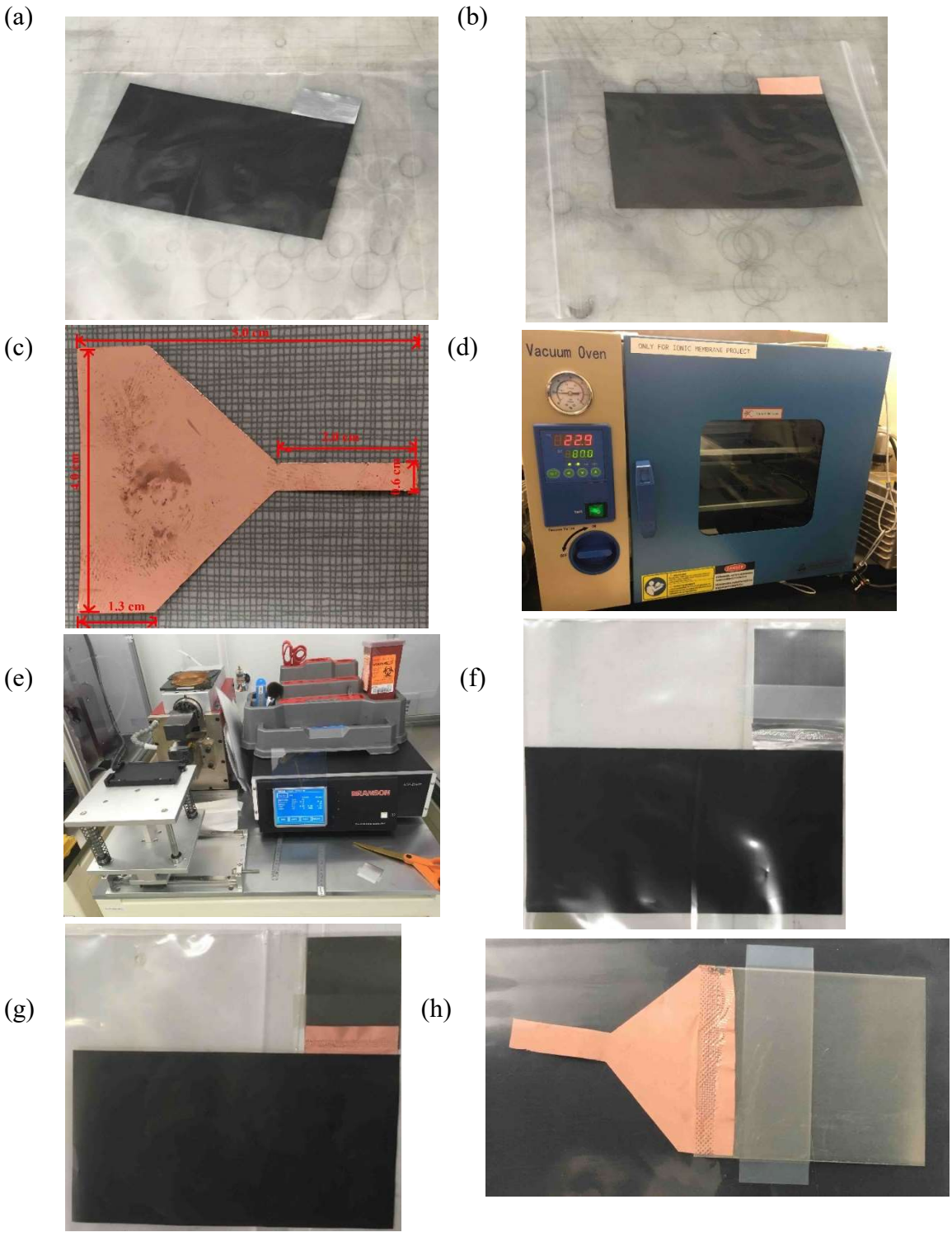

Figure 2-2 Pouch cell electrode material and preparation equipment

(a) cathode (b) anode (c) reference shape (d) vacuum oven (e) welding machine (f) cathode with tab (g) anode with tab (h) reference with tab

(a)

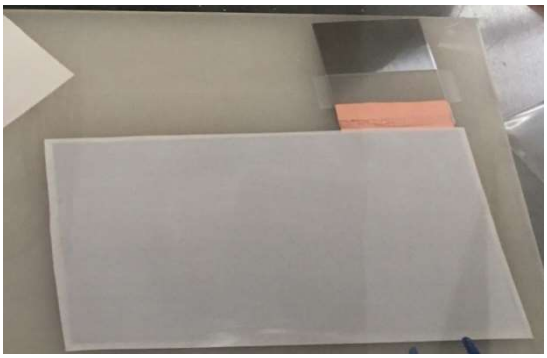

(b)

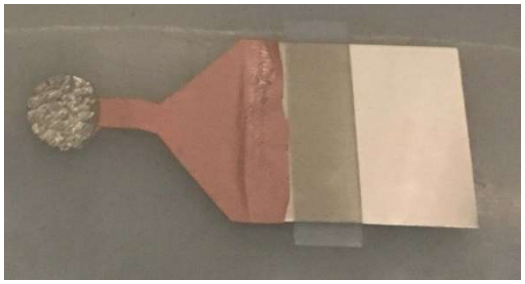

(c)

(d)

(e)

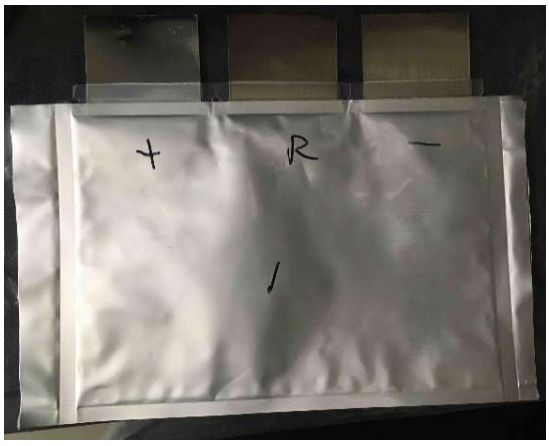

Figure 2-3 Pouch cell sealing process

(a) anode taped with separator (b) lithium foil reference electrode (c) assembled electrode core

(d) sealing machine (e) well-done pouch cell

2.3. Cell testing

2.3.1. Coin cells

The cycling performance of the coin cells containing different electrolytes were measured using custom built Arbin Battery tester (shown in Figure 2-4 Cells testing (a)). The procedures were designed to represent the battery duty cycles in a micro-hybrid vehicle. Each coin cell had the theoretical total capacity of 1.49 mAh.

First, the cells were charged by constant current of C/20 rate until the voltage reached 4.1 V. Then the voltage was held constant at 4.1 V until the current value decayed to the C/20 rate. The cells were then discharged at a constant current of C/20 rate until the voltage decreased to 2.0 V. This process was done for two cycles. Then, a constant current constant voltage charge/discharge cycle at a rate of C/10 were applied between 2.0 V and 4.1 V for three cycles. Between each charge and discharge cycle a one-minute rest period was given. The entire formation process was completed at 25℃, controlled by a temperature chamber (shown in Figure 2-4 (b)).

After the completion of the formation, the cells were charged with 1C rate at 25℃ and then cooled to -20℃ for 2 hours and then discharged at a 5C rate.

The cells were then warmed to 25℃ and allowed to stay at this temperature overnight. These cells were then held at 25℃ and cycled for 50 cycles at a 1C charge and 5C discharge rate. At the end of the 50 cycles, the -20℃ discharge cycle was repeated.

The cells were then warmed to 25℃ again, and then held at 60℃ and cycled for another 50 cycles at a 1C charge and 5C discharge rate. At the end of the high temperature 50 cycles, the -20℃ discharge cycle was repeated to measure the cold temperature performance.

2.3.2. Pouch cells

Before cycling the pouch cell, the impedance was measured using an Autolab potentiostat at 25℃ (shown in Figure 2-4 (c)). In the three-electrode pouch cell, the anode impedance, cathode impedance and full cell impedance were measured individually. The impedance measurement was performed in the galvanotactic mode. The frequency ranged from 100 KHz to 100 mHz, the current was controlled to 0 A with the amplitude of 0.1 A.

After taking the impedance before any cycles, the pouch cell formation was conducted using custom built Arbin Battery testing equipment. The formation was done exactly as described above for the coin cells.

After formation. The pouch cells were charged to 100% state of charge (SOC), at a rate of 1C at 25℃. After resting for 2 hours, the impedance was taken at 25℃. Then, the cells were put at -20℃ for 3 hours and the impedance was taken again at -20℃.

The cells were warmed at 25℃ for 8 hours, then were discharged to 2.0 V at the rate of C/10 (i.e. fully discharge state). After a one-minute rest, the cells were charged to 50% SOC at the rate of 1C at 25℃. After that, the impedance was taken at 25℃ and -20℃ as described above.

This same procedure was repeated at 30% SOC.

After the pouch cell was fully discharge to 2.0 V at the rate of C/10, they were held at 25℃ and cycled for 50 cycles at a 1C charge and 5C discharge rate. At the end of the 50 cycles, the impedance was taken at 100% SOC, 50% SOC and 30% SOC both at 25℃ and -20℃ as described above.

The cold cells were warmed at up to room temperature. After being discharges, they were held at 60℃ and cycled for another 50 cycles at a 1C charge and 5C discharge rate. After this high temperature cycling, the impedance was taken again at 100% SOC, 50% SOC and 30% SOC both at 25℃ and -20℃ as described above.

(a)

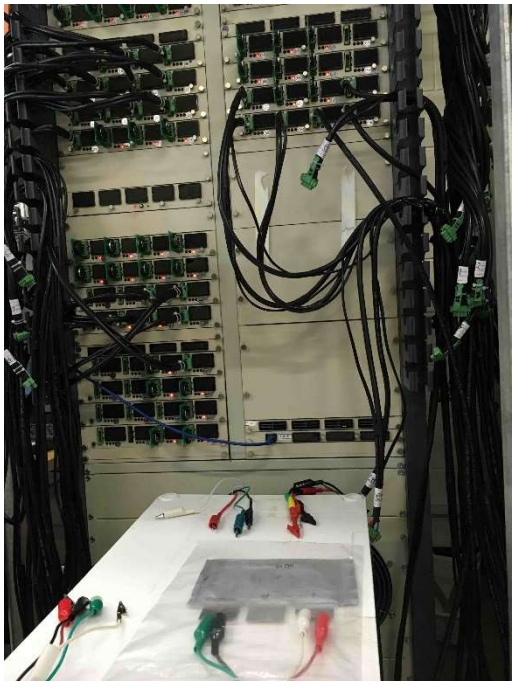

(b)

(c)

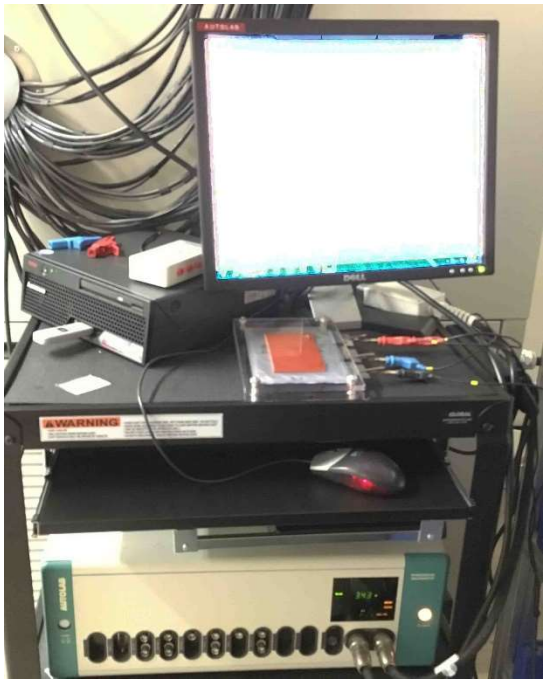

Figure 2-4 Cells testing equipment

(a) Arbin Battery testing equipment (b) Temperature chamber (c) Autolab equipment

3. Results and discussion

3.1. Cycling performance

3.1.1. Coin cell and pouch cell

A series of coin cells and pouch cells cycling results were compared using the same Baseline electrolyte initially.

Figure 3-1 shows the charging discharging curves for the formation process of both coin cells and pouch cells. The voltage is plotted against the time. The first two curves represent the C/20 charge/discharge cycles, while the last three represent the C/10 cycles. Even though the charging process is constant current and constant voltage, Figure 3-1 hardly shows any plateau at 4.1 V which represents the constant voltage charging. It indicates that C/20 and C/10 charging rate are slow enough to lead both the coin cell and the pouch cell to the fully charged state. The charge/discharge curves shape of pouch cell and coin cell are the same. The offsets of last three peaks between pouch and coin cell are not significant, which means after two formation cycles, the pouch cell has a similar response to the C/10 rate charge/discharge as that of the coin cell.

The cycling performance was tested for both coin cells and pouch cells. The active areas were different between coin cell and pouch cell. Therefore, a discharge capacity per unit area was calculated. A comparison of the performance of the coin cells and pouch cells is shown in Figure 3-2.

According to Figure 3-2, during the formation cycle, the pouch cell discharge capacity is 1.54% less than that of the coin cell. It indicates that there is no major difference of the discharge capacities between the coin cell and the pouch cell. During the room temperature cycling, the

capacities drop both in coin cells and pouch cells because the rate increased from C/10 to 5C (the difference in capacity raises to 19.21%). The standard deviation of discharge capacity during room temperature cycles is 0.0125 mAh/cm^2 for pouch cell and 0.0190 mAh/cm^2 for coin cell. The small value of deviation infers a high level of reproducibility for both pouch cells and coin cells at room temperature. During the high temperature cycling, the rate was 5C, and the pouch cell capacity is 15.61% less than coin cell capacity. The discharge capacities of both cells decrease with cycling under high temperature. The decreasing slopes are similar between the pouch cell and the coin cell.

The comparison of cycling performance exhibits the similarity of the pouch cell and coin cell. From this, it can be assumed that the electrolytes behave similarly in both coin cells and pouch cells. The impedance growth can be also predicted to behave similarly in coin cells and pouch cells. The discharge capacity of pouch cell is lower than that of the coin cell. The reason for this might be due to some errors during the pouch cell assembly or the large size of the electrodes. Since, the electrode preparation process could introduce some errors and the errors might have been amplified with larger electrodes.

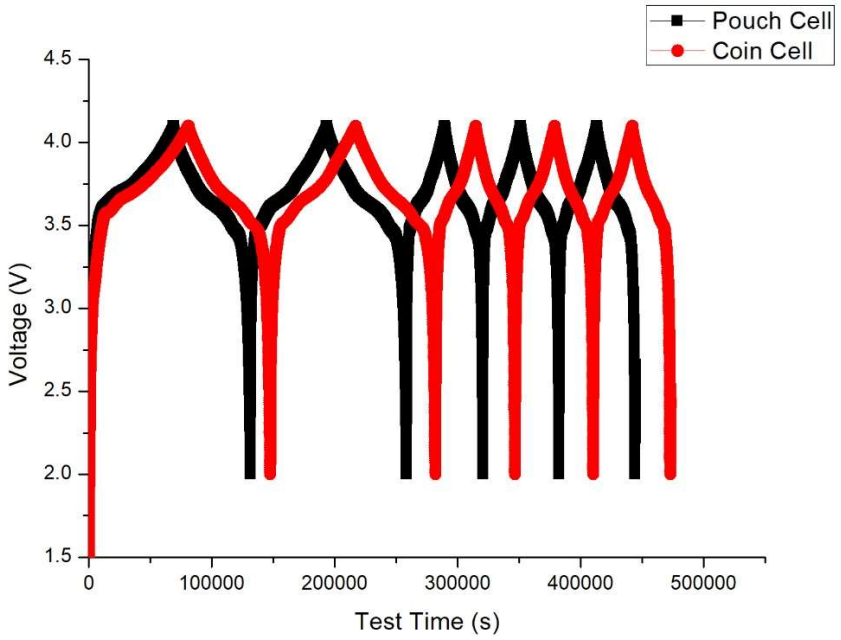

Figure 3-1 Voltage vs. time plot during formation process

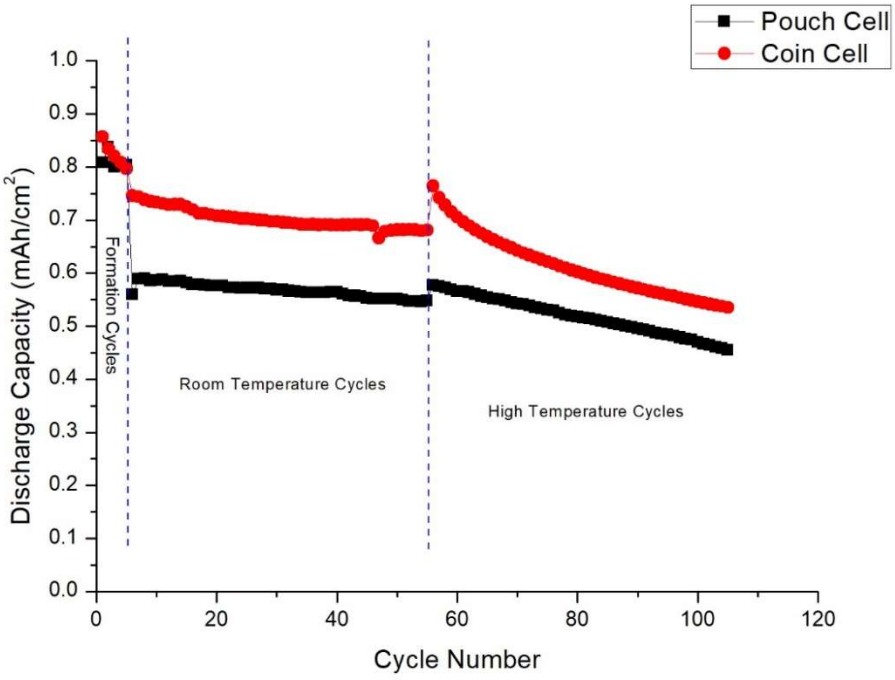

Figure 3-2 Discharge capacity vs. cycle number plot

3.1.2. Baseline electrolyte and improved electrolyte

The comparison of discharge performance at room temperature and low temperature between Baseline electrolyte and improved electrolyte was performed using coin cells.

Figure 3-3 shows the 5C rate discharge curve at room temperature. The voltage curves for baseline electrolyte and improved electrolyte have a similar shape. The ending point (on the x-axis) represents the total discharge capacity. The improved electrolyte has a 0.22% larger capacity than the baseline. It can be concluded that there is no significant difference between the discharge performance of the baseline electrolyte and the improved electrolyte at room temperature.

Figure 3-4 shows a comparison of discharge curves at -20℃ between the cell containing the baseline electrolyte and the improved electrolyte right after formation. It can be seen that at -20℃ with a 5C discharge rate, the improved electrolyte gives 23.44% more discharge capacity than that of the Baseline electrolyte. After 50 cycles at room temperature, the difference in discharge performance becomes larger. In Figure 3-5, it shows that improved electrolyte can produce 87.91% more capacity (discharge) compared to the baseline electrolyte. Figure 3-6 shows that, after another 50 cycles at 60℃, the baseline electrolyte gives a very small discharge capacity at -20℃. However, the improved electrolyte still provides 0.339 mAh/cm^2 capacity (discharge) which is 3.4 times greater than that of the Baseline electrolyte.

Another conclusion can be obtained by looking at the individual electrolytes. Table 3-1 shows how the discharge capacity decayed at low temperature. The two electrolytes started from the same discharge capacity level at room temperature at a 5C discharge rate. The fresh cell with improved electrolyte keeps 71.02% capacity at -20℃ and keeps 62.67% capacity when

discharging after 50 room temperature cycles. After another 50 cycles at high temperature, it still delivers 47.47% of its capacity at -20℃. However, Baseline electrolyte has only 57.66%, 33.42% and 10.78% capacity after formation, room temperature cycles and high temperature cycles respectively.

Table 3-1 Discharge capacity at 5C in different conditions (mAh/cm^2)

	Room Temp.	-20℃ after formation	-20℃ after room Temp. cycles	-20℃ after high Temp. cycles
Baseline	0.713	0.411	0.238	0.077
Improved	0.714	0.507	0.448	0.339

It can be concluded that the improved electrolyte has the similar cycling performance with Baseline electrolyte at room temperature. However, the low temperature discharge experiments indicate that improved electrolyte can deliver larger discharge capacities at -20℃ and maintain its capacity better after high temperature cycling than the baseline electrolyte.

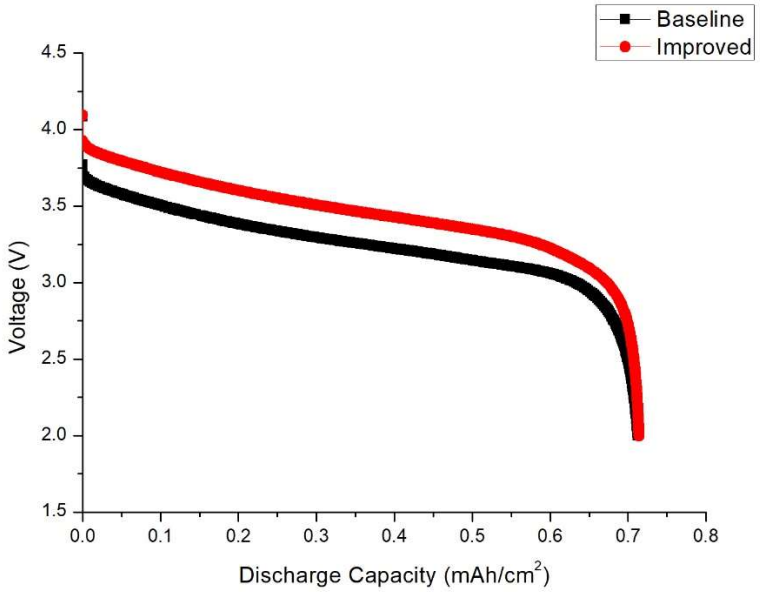

Figure 3-3 Discharge curve of the cells containing baseline and improved electrolytes at 25˚C (5C rate)

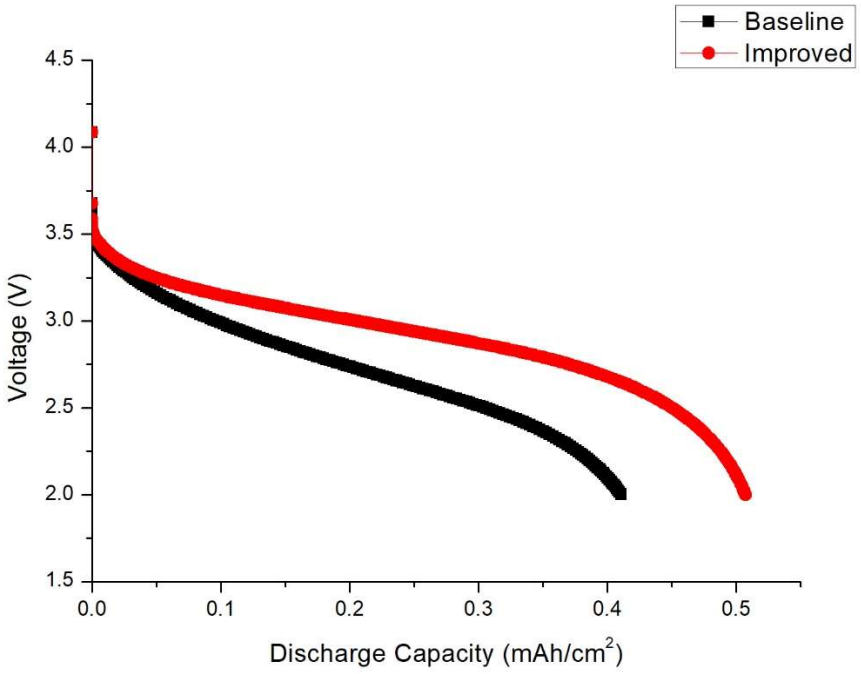

Figure 3-4 Discharge curve of the cells containing baseline and improved electrolytes at -20˚C (5C rate) after formation

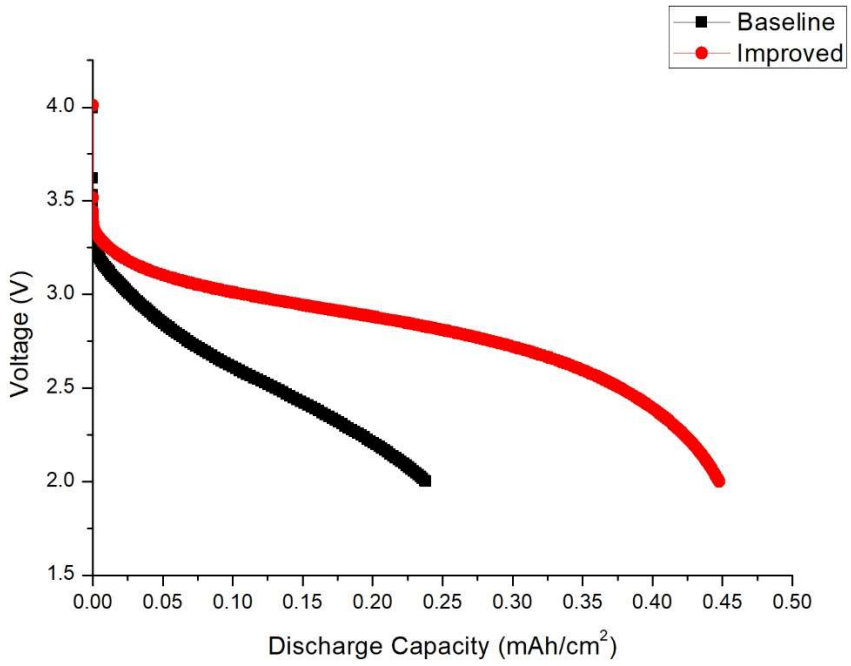

Figure 3-5 Discharge curve of the cells containing baseline and improved electrolytes at -20˚C (5C rate) after 50 cycles at 25˚C

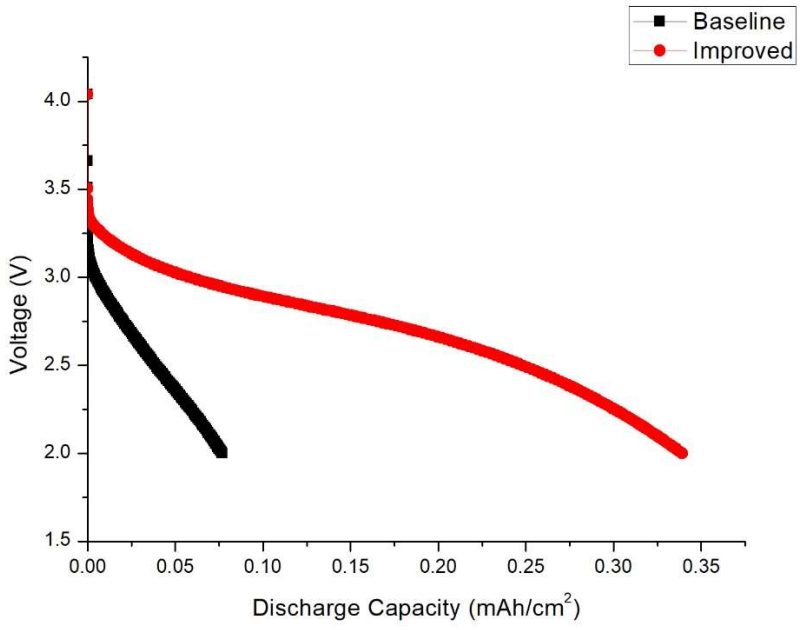

Figure 3-6 Discharge curve of the cells containing baseline and improved electrolytes at -20˚C (5C rate) after 50 cycles at 60˚C

3.2. Impedance results

3.2.1. Quality of the data

The impedance response was measured in a three-electrode pouch cell configuration. Due to the complexity of lithium-ion batteries, the system may deviate from the ideal linear and stationary conditions which are required for accurate modelling. In other words, a reliable impedance spectrum needs four conditions: causality, linearity, stability and finiteness [33]. For example, the excitation signal should be balanced, so that it doesn't drive the battery system from the region of linearity, but large enough to ensure accuracy. It may take a relatively longer rest time for the system to reach stability since electrodes in a Li-ion battery are made with porous materials which results in long relaxation times. Therefore, it is important to make sure the obtained impedance data are reliable and representative to ensure the accuracy of the subsequent equivalent circuit modeling. A Kramers-Kronig (K-K) relationship [45] is commonly used to support the validity of the quality of impedance data at each frequency. Theoretically, for a stable system, the real and imaginary parts of the impedance are interdependent In other words, the real part of an impedance can be obtained by direct integration of K-K equations and vise verse. The K-K equations are listed below:

$$Z'(\omega) = \lim_{\omega \to \infty} [Z'(\omega)] + \left(\frac{2}{\pi}\right) \int_0^{\infty} \frac{xZ''(x) - \omega Z''(\omega)}{x^2 - \omega^2} dx \quad (3\text{-}1)$$

$$Z''(\omega) = \left(\frac{2\omega}{\pi}\right) \int_0^{\infty} \frac{Z'(x) - Z'(\omega)}{x^2 - \omega^2} dx \quad (3\text{-}2)$$

The calculated real (from imaginary) and calculated imaginary (from real) can then be compared with the experimental results. The divergence between the calculated impedance and experimental ones should be low enough to ensure the stability of the system and validity of the

data. It is worth to pointing out that integration over the frequency range from zero to infinity is needed to perform the K-K transformation. While an impedance measurement is always performed in a limited range of frequencies, approximation must be used for the frequencies outside the experimental ranges. An extrapolation to zero and an infinite frequency was performed since the data points can only cover a finite frequency range [46]. On the other hand, the experimental data are fitted to a Voigt circuit (shown in Figure 1-2). If the data can be fitted with satisfaction, they can be considered as K-K compliant [47]. However, with enough R-C elements, a Voigt circuit may fit any spectrum, which is a major limitation of the method. ZView was used for K-K calculation, in which the equivalent model was used to calculate the impedance response outside of the measured frequency range.

The K-K validation is specifically critical to battery systems. Because of the highly porous nature of battery electrodes, it takes a very long time for a battery to reach true stable state. Therefore, the "stability" of a battery system would be related to the frequency of the excitation signal. Figure 3-7 shows the K-K validation of two typical impedance data from the research. Figure 3-7 (a) shows the spectrum of K-K compliance, while Figure 3-7 (b) shows the K-K non-compliant impedance spectrum. In the figures, the circles are experiment data; solid lines are the least square fitting based on the equivalent circuit shown in the corresponding inserts; while the triangles are the impedance spectrum based on K-K calculation (real impedance was calculated from imaginary and vise verse using equations 3-1 and 3-2). It is clearly shown in Figure 3-7 (a) that even if spectrum was K-K compliant, the errors at different frequency ranges varied. Another observation needs to be pointed out is that an apparent good fit can be achieved even through the data were not K-K compliant, as shown in Figure 3-7 (b). This could lead to misinterpreting data using equivalent circuit fitting for an impedance spectrum.

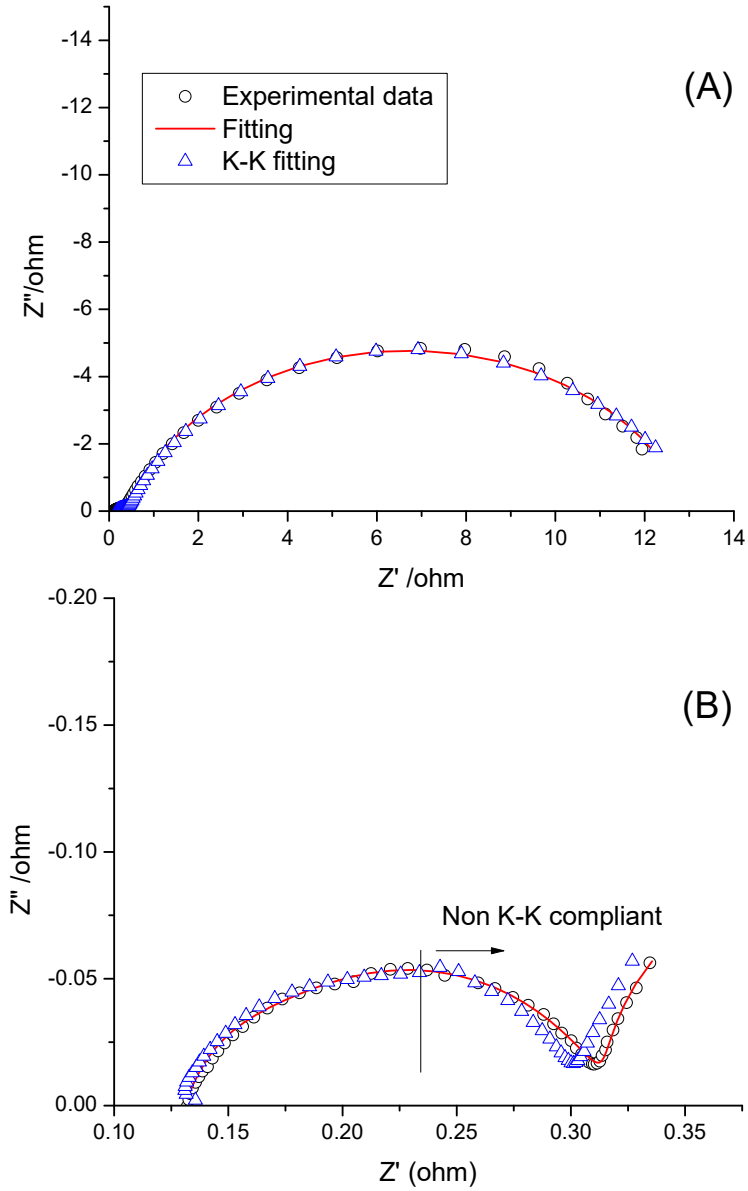

Figure 3-7 Numerical fitting and K-K fitting of typical impedance spectrum

(a)

3.2.2. Building equivalent circuit through the distribution of relaxation times

B

y

a

p

p

l

y

i

n

g

e

q

u

a

t

i

o

n

The data was collected from a three-electrode pouch cell after formation at 100% SOC. The impedance spectrum was measured at room temperature and -20℃. The left side of Figure 3-8 shows the comparison of the impedance spectrum of the cells made with baseline electrolyte and that of the improved electrolyte at 25℃ and -20℃, while the corresponding DRTs are also shown in the right side of Figure 3-8.

R

E

F

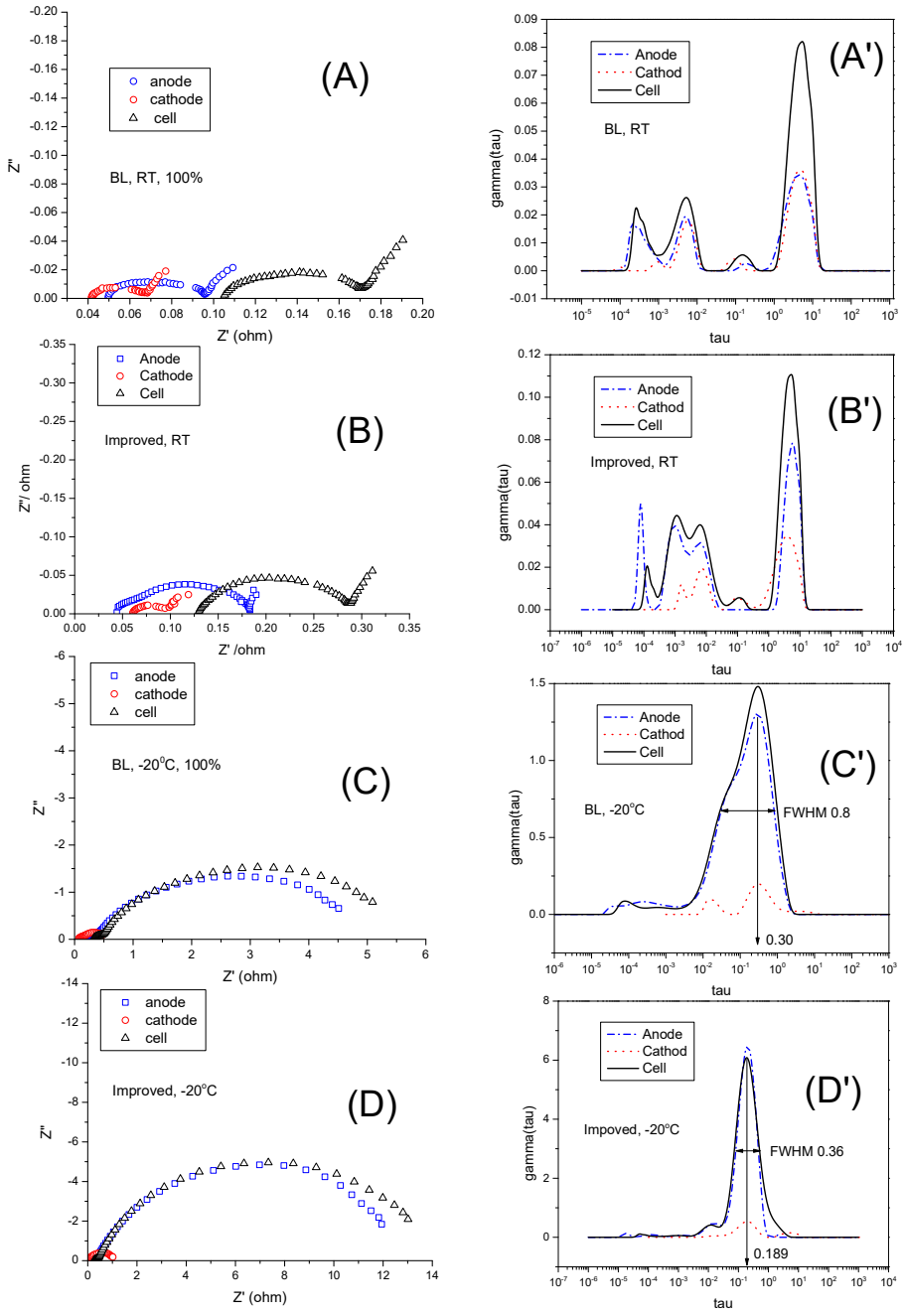

Figure 3-8 The comparison of the impedance spectrum and DRT

(A) and (A'): baseline (BL) electrolyte at room temperature (RT); (B) and (B'): improved electrolyte at RT; (C) and (C'): BL electrolyte at -20°C; (D) and (D'): improved electrolyte at -20°C.

The DRT offers direct access to the rate constants (relaxation times) of each physical and electrochemical process from the impedance spectrum, so do the relaxation amplitudes (polarization resistances), which can be calculated by the integration of the corresponding peaks. Although the DRT is calculated using a universal transmission line model with no physical representation for the system under investigation, the DRT can be used to separate the impedance-related physical processes and can undeniably assist the identification of such processes. For example, as shown in Figure 3-8 (A) and (A'), with the baseline electrolyte, the anode has three significant processes, while the cathode has two significant processes. Both the cathode and anode play important roles when operated at 25℃. The limitations for the electrodes in the improved electrolyte at room temperature are similar to the baseline. The cathode processes in the improved electrolyte were almost identical to those in the baseline electrolyte, while the processes in the anode in the improved electrolyte were more complex than those in the baseline electrolyte. Significant differences can be observed for the cells at -20℃. It was interesting that the two processes for the cathodes at -20℃ were about the same as those at room temperature, although the relaxation time (rate constants) changed. The most important observation was that, unlike at room temperature where the both cathode and anode made fair contributions to the cell impedance, the anode processes made the dominant contribution to the cell impedance at -20℃, and only two apparent processes can be identified, which is consistent with the previous work in our group [20].

DRT is based on a universal transmission line model in which the specific nature of the processes are not taken into consideration, it only reveals the kinetic aspects of the processes. The remaining challenge, of course, is to identify the processes and correlate them to the kinetic characteristics. Figure 3-9 shows the equivalent circuit developed through DRT. The equivalent

circuit shown in Figure 3-9 consist of two R/C (CPE) loops representing the two processes revealed in DRT. The R_{ct}/C represents the interfacial charge transfer reaction resistance and double-layer capacitance between the anode and SEI layer. The CPE/R represents the lithium ion diffusion in a non-uniform SEI and with the graphite lattice. The ohmic resistance (R_s) consists of the electronic resistance e.g. contact resistance between particles and current collectors, and ionic resistance e.g. electrolyte resistance. The solid line in Figure 3-9 shows the excellent fitting for the impedance spectrum.

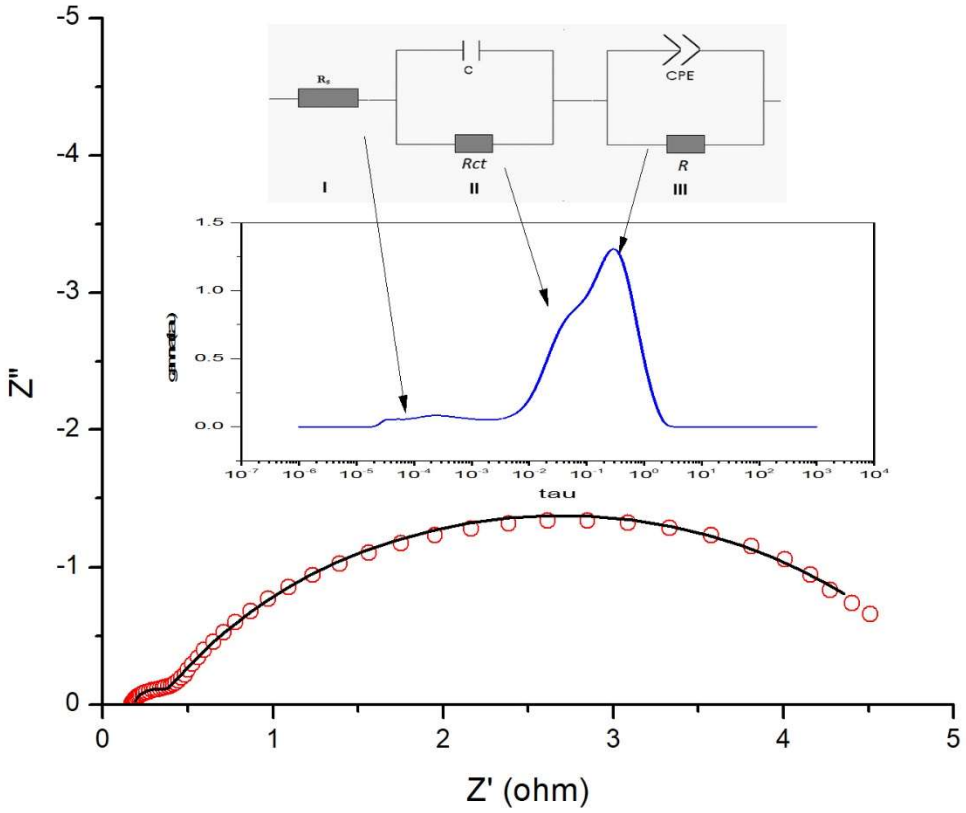

Figure 3-9 Building the equivalent circuit based on DRT

3.2.3. Fitting the experimental impedance spectrum at -20°C

Figure 3-10 shows the comparison of experimental data and the fitting curves for the anode in both the baseline electrolyte and the improved electrolyte based on the equivalent circuit shown Figure 3-9. The fitting parameters are tabulated in Table 3-2. As demonstrated, the fitting errors were almost all below 10%.

Table 3-2 Equivalent fitting results for the impedance spectrum shown in Figure 3-10

	R_s(Ω)	**C (mF)**	**R_{ct} (Ω)**	**R (Ω)**	**CPE-T**	**CPE-P**
Baseline	0.18 (0.8%)	0.86 (3.2%)	0.14 (2.3%)	4.7 (1.2%)	0.06 (1.8%)	0.87 (5.4%)
Improved	0.201 (8%)	0.8 (3.3%)	0.2 (10.4%)	12.6 (0.3%)	0.01 (0.53%)	0.63 (5.3%)

The three-electrode pouch cell results echoed those of our previous coin cell results [20]. For example, the conductivity of electrolyte played a minor role in the low temperature performance and the major contribution to the cell impedance was from anode instead of cathode. In addition, the interfacial charge transfer reaction was similar for both electrolytes as shown in Table 3-2.

Interestingly, conventional wisdom has taught us that an electrode showing a large semi-circle would have worse rate capability than that with smaller semi-circle. Apparently, this hypothesis is not correct in this case. As shown in Figure 3-10, the semi-circle of the impedance for the anode in the improved electrolyte was substantially larger than that of the baseline electrolyte. Indeed, the R value of the improved electrolyte is significant higher than that of the baseline electrode (Table 3-2). DRT peaks shown in Figure 3-8 may provide the explanation for these phenomena. Comparing DRT graphs in Figure 3-8 baseline electrolyte (C') and improved

electrolyte (D'), although the peak area in (C') was significant larger than that of (D'), the peak position of the major peak in (D') (0.19) was at a lower relaxation time than that of (C') (0.3); the full width at half maximum (FWHM) of (D') (0.36) was also smaller than that of (C') (0.80). Therefore, although the polarization resistance of the processes for the anode in baseline was smaller, the kinetics for the processes were more sluggish for the anode in the baseline electrolyte. Indeed, the two major processes for the anode in the improve electrolyte can be clearly separated while they overlapped for that of baseline electrode (Figure 3-8 (C') and (D')). A CPE-P element is used to model the diffusion in a distributed a non-homogeneous matrix (e.g. the matrix with wide pore size distribution). For the diffusion in a homogenous matrix, CPE-P is equal to 0.5, the well-known 45-degree line shows on the Nyquist plot and 1/CPE-T is proportional to the diffusion coefficient. The deviation of CPE-P from 0.5 illustrates the degree the system deviates from its homogeneity. The CPE/R loop in the equivalent circuit (Figure 3-9) was used to simulate the ionic diffusion in the non-homogeneous and porous SEI layer. Table 3-2 tabulates the fitting results for the two electrodes. The CPE-P for the anodes in the baseline electrolyte and in the improved electrolyte were 0.87 and 0.63, respectively, with the CPE-P from the baseline electrolyte deviated away from 0.5 more than that of the improved electrolyte. It demonstrated that the nature of the SEI layers of the anode in the baseline electrolyte is more non-homogenous. Consequently, the CPE-T for the improve electrolyte (0.01) was small than that of the baseline electrolyte (0.06), or the lithium diffusion coefficient in the SEI layer in improved electrolyte was substantially higher than that in the baseline electrolyte. The conclusions were in agreement with those in our previous work [20].

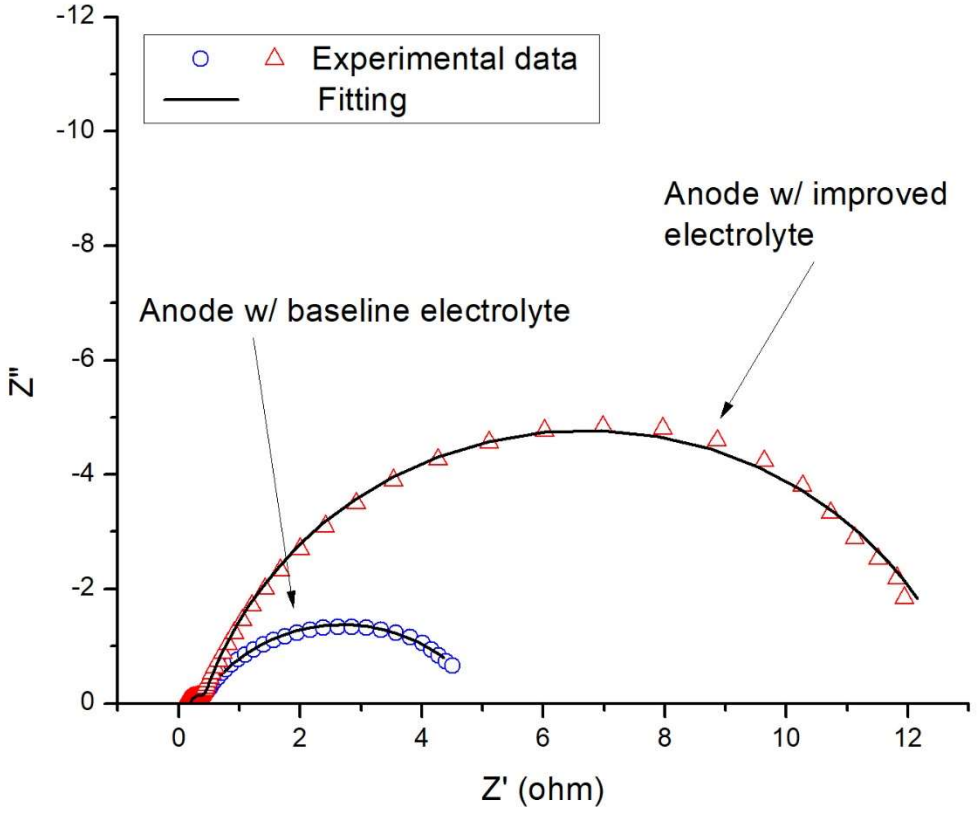

Figure 3-10 Impedance spectrum and their fittings for the anodes in both baseline electrolyte and improved electrolyte at -20℃

4. Conclusion

The cycling results exhibit that discharge capacity at -20℃ of the improved electrolyte is significantly better than that of the baseline electrolyte. Comparing the cycling performance at different temperature, the electrolytes in the designed three-electrode pouch cells work similarly to those in coin cells.

The impedance results in a three-electrode pouch cell clearly demonstrated that the determining factor for the low temperature performance is on the graphite anode. Using DRT, the relaxation time (rate constant) for the electrode processes can be revealed from the impedance spectrum. Combining DRT and equivalent circuit fitting, the homogeneity of the SEI layer on the surface of the anode plays an important role. In addition, Li-ion diffusion kinetics through the SEI layer is more influential than the actual polarization resistance to the low temperature performance of the graphite anode.

5. Future work

In this thesis, only the impedance results after formation of the cells at a 100% SOC at room temperature and -20℃ were discussed. Further studies of AC-impedance after different types of aging cycles (i.e. after 50 cycles at room temperature and after another 50 cycles at 60℃) and at different SOC (i.e. 50% and 30%) would lead to a deeper understanding of the electrolytes differences. This could lead to greater knowledge of how the SEI grows after aging and how the electrochemical process changes at different SOC.

Two electrolyte systems were compared in this work. A further investigation could involve more than two electrolyte systems. By changing one of the electrolyte components or changing several components systematically, how the different components affect the SEI formation could be investigated through EIS.

The three-electrode pouch cell making procedure still could be further optimized. By utilizing a custom die in the sealing machine, a smaller three-electrode pouch cell could be made. It might reduce the errors in the cycle performance by decreasing the size of the electrodes.

EIS is not the only powerful method to investigate the surface properties of lithium-ion battery electrode (i.e. SEI). A further study on SEI could combine different techniques. For example, using SEM, the surface quality of the electrode could be visually evaluated. Through a high-resolution SEM picture, the SEI structure could even be distinguished. XPS is another method to analyze the SEI. The different elements and different function groups on the electrode surface could be identified through XPS. Those techniques will be considered in any future work aimed at investigating the SEI layer formation in a lithium-ion battery.

REFERENCES

[1] D. Linden, Handbook of batteries, in Fuel and Energy Abstracts, 1995, vol. 4.

[2] M. Bellis, Meet the Inventor of the First Battery, ThoughtCo. Available: https://www.thoughtco.com/alessandro-volta-1992584. [Accessed: 09-Jul-2018].

[3] J.-M. Tarascon and M. Armand, Issues and challenges facing rechargeable lithium batteries, Materials For Sustainable Energy: A Collection of Peer-Reviewed Research and Review Articles from Nature Publishing Group, World Scientific, 2011, pp. 171–179.

[4] S. Basu, C. Zeller, Synthesis and properties of lithium-graphite intercalation compounds, Materials Science and Engineering, vol. 38, no. 3, pp. 275–283, 1979.

[5] R. Yazami, A reversible graphite-lithium negative electrode for electrochemical generators, Journal of Power Sources, vol. 9, no. 3, pp. 365–371, 1983.

[6] N. A. Godshall, I. D. Raistrick, Thermodynamic investigations of ternary lithium-transition metal-oxygen cathode materials, Materials Research Bulletin, vol. 15, no. 5, pp. 561–570, 1980.

[7] K. Mizushima, J. B. Goodenough, LixCoO2: for batteries of high energy density, Materials Research Bulletin, vol. 15, no. 6, pp. 783–789, 1980.

[8] Z. Lu, J. R. Dahn, Cathode compositions for lithium-ion batteries, US6964828B2, 15-Nov-2005.

[9] H. Yoshizawa, T. Ohzuku, An application of lithium cobalt nickel manganese oxide to high-power and high-energy density lithium-ion batteries, Journal of Power Sources, vol. 174, no. 2, pp. 813–817, 2007.

[10] K. Xu, Nonaqueous Liquid Electrolytes for Lithium-Based Rechargeable Batteries, Chemical Reviews, vol. 104, no. 10, pp. 4303–4418, 2004.

[11] G. J. Janz, Nonaqueous electrolytes handbook, vol. 1. Elsevier, 2012.

[12] M. Ue, Mobility and Ionic Association of Lithium and Quaternary Ammonium Salts in Propylene Carbonate and γ-Butyrolactone, J. Electrochem. Soc., vol. 141, no. 12, pp. 3336–3342, 1994.

[13] K. Naoi, M. Mori, The Surface Film Formed on a Lithium Metal Electrode in a New Imide Electrolyte, Lithium Bis(perfluoroethylsulfonylimide) [$LiN(C_2F_5SO_2)_2$], J. Electrochem. Soc., vol. 146, no. 2, pp. 462–469, 1999.

[14] H. Yang, K. Kwon, Aluminum Corrosion in Lithium Batteries an Investigation Using the Electrochemical Quartz Crystal Microbalance, J. Electrochem. Soc., vol. 147, no. 12, pp. 4399–4407, 2000.

[15] G. Pistoia, M. D. Rossi, Study of the Behavior of Ethylene Carbonate as a Nonaqueous Battery Solvent, Journal of The Electrochemical Society, vol. 117, no. 4, p. 500, 1970.

[16] J. R. Dahn, Studies of Lithium Intercalation into Carbons Using Nonaqueous Electrochemical Cells, J. Electrochem. Soc., vol. 137, no. 7, pp. 2009–2013, 1990.

[17] J. M. Tarascon, New electrolyte compositions stable over the 0 to 5 V voltage range and compatible with the $Li_{1+x}Mn_2O_4$/carbon Li-ion cells, Solid State Ionics, vol. 69, no. 3, pp. 293–305, 1994.

[18] D. Aurbach, The Study of Electrolyte Solutions Based on Ethylene and Diethyl Carbonates for Rechargeable Li Batteries II. Graphite Electrodes, J. Electrochem. Soc., vol. 142, no. 9, pp. 2882–2890, 1995.

[19] Y. Ein-Eli, S. R. Thomas, Ethylmethylcarbonate, a Promising Solvent for Li-Ion Rechargeable Batteries, J. Electrochem. Soc., vol. 143, no. 12, pp. L273–L277, 1996.

[20] J. Kafle , Development of wide temperature electrolyte for graphite/ $LiNiMnCoO_2$ Li-ion cells: High throughput screening, Journal of Power Sources, vol. 392, pp. 60–68, 2018.

[21] Y. Matsuda, Behavior of lithium/electrolyte interface in organic solutions, Journal of Power Sources, vol. 43, no. 1, pp. 1–7, 1993.

[22] D. Xiong, A High Precision Study of the Effect of Vinylene Carbonate (VC) Additive in Li/Graphite Cells, Journal of The Electrochemical Society, vol. 158, no. 12, p. A1431, 2011.

[23] K. Xu, LiBOB as Salt for Lithium-Ion Batteries:A Possible Solution for High Temperature Operation, Electrochemical and Solid-State Letters, vol. 5, no. 1, p. A26, 2002.

[24] K. Xu, Lithium Bis(oxalato)borate Stabilizes Graphite Anode in Propylene Carbonate, Electrochemical and Solid-State Letters, vol. 5, no. 11, p. A259, 2002.

[25] K. Xu, Formation of the Graphite/Electrolyte Interface by Lithium Bis(oxalato)borate, Electrochemical and Solid-State Letters, vol. 6, no. 6, p. A117, 2003.

[26] A. N. Dey, B. P. Sullivan, The Electrochemical Decomposition of Propylene Carbonate on Graphite, J. Electrochem. Soc., vol. 117, no. 2, pp. 222–224, 1970.

[27] E. Paled, The Electrochemical Behavior of Alkali and Alkaline Earth Metals in Nonaqueous Battery Systems, J. Electrochem. Soc., vol. 126, no. 12, pp. 2047–2051, 1979

[28] J. O. Besenhard, Filming mechanism of lithium-carbon anodes in organic and inorganic electrolytes, Journal of Power Sources, vol. 54, no. 2, pp. 228–231, 1995.

[29] T. Abe, Intercalation of lithium into natural graphite flakes and heat-treated polyimide films in ether-type solvents by chemical method, Journal of Power Sources, vol. 68, no. 2, pp. 216–220, 1997.

[30] M. Inaba, Electrochemical Scanning Tunneling Microscopy Observation of Highly Oriented Pyrolytic Graphite Surface Reactions in an Ethylene Carbonate-Based Electrolyte Solution, Langmuir, vol. 12, no. 6, pp. 1535–1540, 1996.

[31] K. Kanamura, Electrochemical Deposition of Very Smooth Lithium Using Nonaqueous Electrolytes Containing HF, J. Electrochem. Soc., vol. 143, no. 7, pp. 2187–2197, 1996.

[32] G.C. Chung, Origin of Graphite Exfoliation an Investigation of the Important Role of Solvent Countercoalition, J. Electrochem. Soc., vol. 147, no. 12, pp. 4391–4398, 2000.

[33] D. Qu, Electrochemical Impedance and its Applications in Energy-Storage Systems, Small Methods, p. 1700342, 2018.

[34] H. Fricke, The theory of electrolytic polarization, The London, Edinburgh, and Dublin Philosophical Magazine and Journal of Science, vol. 14, no. 90, pp. 310–318, 1932.

[35] T. Pajkossy, Impedance of rough capacitive electrodes, Journal of Electroanalytical Chemistry, vol. 364, no. 1–2, pp. 111–125, 1994.

[36] B.E. Conway, Impedance Spectroscopy: Theory, Experiment, and Applications, New York: Wiley, 2016.

[37] G. Hu, Synthesis and electrochemical properties of $xLiFePO_4 \cdot (1-x)Na_3V_2(PO_4)_2F_3/C$ composite for lithium-ion batteries, Journal of Alloys and Compounds, vol. 696, pp. 177–184, 2017.

[38] G. Nagasubramanian, Two- and three-electrode impedance studies on 18650 Li-ion cells, Journal of Power Sources, vol. 87, no. 1, pp. 226–229, 2000.

[39] T. Osaka, Proposal of novel equivalent circuit for electrochemical impedance analysis of commercially available lithium ion battery, Journal of Power Sources, vol. 205, pp. 483–486, 2012.

[40] T. Momma, T. Osaka, Ac impedance analysis of lithium ion battery under temperature control, Journal of Power Sources, vol. 216, pp. 304–307, 2012.

[41] M. Steinhauer, Investigation of the Solid Electrolyte Interphase Formation at Graphite Anodes in Lithium-Ion Batteries with Electrochemical Impedance Spectroscopy, Electrochimica Acta, vol. 228, pp. 652–658, 2017.

[42] H. Schichlein, Deconvolution of electrochemical impedance spectra for the identification of electrode reaction mechanisms in solid oxide fuel cells, Journal of Applied Electrochemistry, vol. 32, pp. 875–882, 2002.

[43] P. Agarwal, Measurement Models for Electrochemical Impedance Spectroscopy I. Demonstration of Applicability, J. Electrochem. Soc., vol. 139, no. 7, pp. 1917–1927, 1992.

[44] R. M. Fuoss, J. G. Kirkwood, Electrical Properties of Solids. VIII. Dipole Moments in Polyvinyl Chloride-Diphenyl Systems*, J. Am. Chem. Soc., vol. 63, no. 2, pp. 385–394, 1941.

[45] E. Riecke, Physikalische Zeitschrift. S. Hirzel, 1929.

[46] M. Urquidi-Macdonald, Applications of Kramers—Kronig transforms in the analysis of electrochemical impedance data—III. Stability and linearity, Electrochimica Acta, vol. 35, no. 10, pp. 1559–1566, 1990.

[47] P. Agarwal, The influence of error structure on interpretation of impedance spectra, Electrochimica Acta, vol. 41, no. 7, pp. 1017–1022, 1996.

APPENDIX A. Anode impedance date for baseline electrolyte after formation at 100% SOC at -20°C

Frequency (Hz)	Z' (Ω)	-Z'' (Ω)	Z (Ω)
99998.5	0.130593	-0.0138534	0.131325
79431.5	0.124331	-0.00513353	0.124437
63095.1	0.126281	0.00266445	0.126309
50118.4	0.130023	0.0107134	0.130463
39810.2	0.132292	0.0202837	0.133838
31622.9	0.138012	0.0269377	0.140616
25118.8	0.144002	0.0316901	0.147448
19952.8	0.150548	0.0361406	0.154825
15848.6	0.156343	0.0407726	0.161572
12589	0.162818	0.0453079	0.169005
9999.99	0.171003	0.0551505	0.179677
7943.15	0.178257	0.0593604	0.18788
6309.51	0.186634	0.0638338	0.197248
5011.8	0.196514	0.068662	0.208164
3980.99	0.206852	0.0743921	0.219822
3162.21	0.218298	0.079741	0.232406
2511.86	0.231683	0.0854004	0.246921
1995.27	0.245362	0.0905532	0.261539
1584.92	0.259575	0.0950512	0.276431
1258.91	0.273402	0.100487	0.291284
999.987	0.291289	0.1031	0.308996
794.321	0.307054	0.106488	0.324996
630.96	0.323555	0.110122	0.341782
501.186	0.339917	0.113251	0.358287
398.107	0.354914	0.116449	0.37353
316.225	0.36956	0.121559	0.389039
251.189	0.383399	0.127111	0.403921
199.53	0.397058	0.135534	0.419553
158.489	0.409518	0.145143	0.434478
125.889	0.422733	0.159509	0.451825
99.9998	0.435912	0.179032	0.471245
79.4325	0.45171	0.203126	0.49528
63.0952	0.466923	0.235539	0.522968

50.1191	0.488891	0.270772	0.558867
39.8103	0.515278	0.317125	0.605045
31.6231	0.544997	0.371586	0.65962
25.1182	0.584475	0.438617	0.73075
19.9527	0.642394	0.509748	0.82007
15.8483	0.704426	0.595605	0.922476
12.5887	0.782597	0.691336	1.04422
9.99984	0.880507	0.798205	1.18845
7.94302	0.998544	0.908514	1.35
6.30959	1.13777	1.02114	1.52881
5.0118	1.30284	1.13313	1.72666
3.98105	1.4872	1.2396	1.93608
3.16225	1.69667	1.34119	2.16275
2.51189	1.92664	1.43383	2.40163
1.99524	2.17898	1.521	2.65732
1.58494	2.44368	1.59371	2.91745
1.25892	2.72463	1.65555	3.18817
1.00001	3.01822	1.69457	3.46139
0.794331	3.31834	1.71792	3.73666
0.630956	3.63521	1.71757	4.02055
0.501183	3.94542	1.68868	4.29161
0.398104	4.2579	1.62793	4.55849
0.316228	4.54324	1.53003	4.79396
0.251188	4.81353	1.41573	5.0174
0.199529	5.04393	1.28176	5.20424
0.158489	5.21222	1.13265	5.33387
0.125889	5.29615	0.980477	5.38615
0.0999989	5.36495	0.850618	5.43197

APPENDIX B. Anode impedance date for improved electrolyte after formation at 100% SOC at -20°C

Frequency (Hz)	Z' (Ω)	-Z'' (Ω)	Z (Ω)
99998.5	0.117699	-0.011614	0.11827
79431.5	0.122106	-0.00238836	0.122129
63095.1	0.115643	0.0104242	0.116112
50118.4	0.122532	0.0161192	0.123587
39810.2	0.128156	0.0286735	0.131324
31622.9	0.13469	0.0357341	0.139349
25118.8	0.142656	0.0427698	0.148929
19952.8	0.150828	0.0474048	0.158102
15848.6	0.15886	0.0524969	0.167309
12589	0.167649	0.0565147	0.176919
9999.99	0.178007	0.0664746	0.190014
7943.15	0.187368	0.0700032	0.200018
6309.51	0.198566	0.0741714	0.211967
5011.8	0.209738	0.0791106	0.224161
3980.99	0.221646	0.0825184	0.236508
3162.21	0.234478	0.0863587	0.249875
2511.86	0.247727	0.0904448	0.263722
1995.27	0.261391	0.0938454	0.277727
1584.92	0.275189	0.0971727	0.291841
1258.91	0.289757	0.102649	0.307402
999.987	0.303301	0.104774	0.320888
794.321	0.315989	0.108697	0.334161
630.96	0.329802	0.113569	0.348808
501.186	0.342471	0.120431	0.363029
398.107	0.35403	0.128906	0.376768
316.225	0.366463	0.141159	0.39271
251.189	0.379098	0.156305	0.410057
199.53	0.391441	0.175081	0.428812
158.489	0.404249	0.200693	0.451326
125.889	0.421089	0.231511	0.480534
99.9998	0.437892	0.269609	0.514236
79.4325	0.458247	0.316901	0.55715
63.0952	0.484691	0.377266	0.614211

50.1191	0.512948	0.44239	0.677366
39.8103	0.549743	0.5262	0.760988
31.6231	0.594185	0.626178	0.863223
25.1182	0.649728	0.743906	0.987695
19.9527	0.724837	0.878662	1.13905
15.8483	0.809614	1.04148	1.31915
12.5887	0.914359	1.23168	1.53397
9.99984	1.04378	1.4513	1.78766
7.94302	1.20683	1.7089	2.09208
6.30959	1.41528	2.00007	2.45017
5.0118	1.67519	2.33041	2.87003
3.98105	1.99982	2.69813	3.35845
3.16225	2.41031	3.09188	3.92037
2.51189	2.9177	3.49934	4.55613
1.99524	3.53705	3.89861	5.26402
1.58494	4.26188	4.26298	6.02799
1.25892	5.10563	4.55981	6.84538
1.00001	6.0169	4.76265	7.67372
0.794331	6.98046	4.83984	8.49417
0.630956	7.96907	4.80639	9.30632
0.501183	8.86127	4.58876	9.97892
0.398104	9.63718	4.23799	10.5279
0.316228	10.2665	3.80079	10.9475
0.251188	10.7284	3.33127	11.2337
0.199529	11.1224	2.88672	11.4909
0.158489	11.5087	2.52303	11.782
0.125889	11.8227	2.18467	12.0228
0.0999989	11.9419	1.84193	12.0831